9,10-Dihydroplatinaanthracenes with Aromatic Diimine Ligands: Syntheses and Spectroscopic and Computational Studies of New Luminescent Materials

Antonio G. De Crisci,[†] Alan J. Lough,[‡] Kanwarpal Multani,[†] and Ulrich Fekl*,[†]

Department of Chemical and Physical Sciences, University of Toronto Mississauga, 3359 Mississauga Road N, Mississauga, Ontario, Canada L5L 1C6, and X-ray Crystallography Lab, University of Toronto St. George, 80 St. George Street, Toronto, Ontario, Canada M5S 3H6

Received October 5, 2007

9,10-Dihydroplatinaanthracenes with aromatic nitrogen ligands were synthesized, derived from 2,2′-bipyridine, 4,4′-dichloro-2,2′-bipyridine, 4,4′-dimethoxy-2,2′-bipyridine, 4,4′-bis(dimethylamino)-2,2′-bipyridine, 4,4′-di-*tert*-butyl-2,2′-bipyridine, 1,10-phenanthroline, 2,9-dimethyl-1,10-phenanthroline, 3,4,7,8-tetramethyl-1,10-phenanthroline, and 2,2′-biquinoline. For comparison purposes, the *N,N,N′,N′*-tetramethylethylenediamine-derived compound was also obtained. A single-crystal X-ray structure determination was carried out on $[H_2C(C_6H_4)_2]$Pt(2,9-dimethyl-1,10-phenanthroline), revealing a pronounced boat conformation of the metallacyclic ring. The diimine-derived compounds are highly luminescent in the solid state at room temperature, as well as in frozen solution. The luminescent complexes are easily prepared by ligand substitution from the new organometallic platinum precursor $\{[H_2C(C_6H_4)_2]Pt(SEt_2)\}_n$ ($n = 2, 3$). Spectroscopic data are provided on absorbance and emission in the UV–visible range. In order to obtain insight into orbital energies and the tunability of the optical properties, electrochemical data, as well as DFT and TD-DFT data, were obtained. The lowest-energy absorbances are due to charge transfer from orbitals located largely on the electron-rich metallacyclic ligand with some coefficient on Pt into π^* orbitals of the diimine. Computations suggest that the low-energy bands mostly originate from charge transfer from the HOMO−2, HOMO−1, and HOMO to the LUMO (rarely LUMO+1 and LUMO+2) molecular orbitals. Emission maxima range from 536 to 690 nm.

Introduction

Metallacycles are important organometallic compounds, and a metallacycle may be defined as "a carbocyclic system with one or more carbons replaced by a transition metal".[1]

Four-membered and five-membered metallacycles are relevant for a host of catalytic cycles leading to C−C bond formation, and while such metallacycles have been studied in much detail in the past, six-membered metallacycles have been studied much less, until, it seems, rather recently.[2] However, an increased amount of research has been directed toward six-membered metallacycles in the last several years, due to the comparably young field of metallabenzenes.[3] A significant part of our research activity aims at synthetically extending the field of six-membered metallacycles involving platinum (platinacycles), and we found the field related to the 9,10-dihydroplatinaanthracenes highly attractive. The first 9,10-dihydroplatinaanthracenes were developed in the pioneering work by Alcock, Bryars, and Pringle,[4] and there exists essentially no published work in this field since the seminal 1990 paper.[5] Co-ligands reported, in addition to the chelating hydrocarbon forming part of the metallacyclic ring, have been alkenes (cyclooctadiene), phosphines, and, for Pt(IV) compounds, additional halides.[4] Surprisingly, no reports are available on nitrogen-based ligands coordinated to 9,10-dihydroplatinaanthracenes. Attaching nitrogen-based aromatic ligands, such as substituted 2,2′-bipyridines or 1,10-phenanthrolines, to a 9,10-dihydroplatinaanthracene promises to provide highly luminescent materials, as might be inferred from the fact that platinum(II) complexes featuring an N_2C_2 coordination sphere have often been found to be luminescent, in particular if the nitrogen donors are part of a π-system. Examples of such luminescent N_2C_2Pt systems are platinum(II) centers bis-chelated by ortho-deprotonated phenylpyridine,[6] platinum(II) bisacetylides having aromatic diimines,[7] monoacetylides containing a cyclometalated 6-phenyl-2,2′-bipyridine,[8] and also diarylplatinum(II) complexes containing as nitrogen donors

* Corresponding author. E-mail: ulrich.fekl@utoronto.ca.
[†] Department of Chemical and Physical Sciences.
[‡] X-ray Crystallography Lab.

(1) Collman, J. P.; Hegedus, L. S.; Norton, J. R.; Finke, R. G. *Principles and Applications of Organotransition Metal Chemistry,* 2nd ed.; University Science Books: Mill Valley, CA, 1987.

(2) (a) Puddephatt, R. J. *Coord. Chem. Rev.* **1980**, *33*, 149. (b) Dyker, G. *Chem. Ber.* **1997**, *130*, 1567. (c) Cámpora, J.; Palma, P.; Carmona, E. *Coord. Chem. Rev.* **1999**, *193–195*, 207.

(3) (a) Bleeke, J. R. *Chem. Rev* **2001**, *101*, 1205. (b) Landorf, C. W.; Haley, M. M. *Angew Chem., Int. Ed.* **2006**, *45*, 3914.

(4) Alcock, N. W.; Bryars, K. H.; Pringle, P. G. *J. Chem. Soc., Dalton Trans.* **1990**, 1433.

(5) However, for a bucky-bowl complex that contains a substructure resembling a *platinaanthracene*: Shaltout, R. M.; Sygula, R.; Sygula, A.; Fronczek, F. R.; Stanley, G. G.; Rabideau, P. W. *J. Am. Chem. Soc.* **1998**, *120*, 835.

(6) Maestri, M.; Sandrini, D.; Balzani, V.; Chassot, L.; Jolliet, P.; von Zelewsky, A. *Chem. Phys. Lett.* **1985**, *122*, 375.

(7) (a) Hissler, M.; McGarrah, J. E.; Connick, W. B.; Geiger, D. K.; Cummings, S. D.; Eisenberg, R. *Coord. Chem. Rev.* **2000**, *208*, 115. (b) Whittle, C. E.; Weinstein, J. A.; George, M. W.; Schanze, K. S. *Inorg. Chem.* **2001**, *40*, 4053. (c) Kang, Y.; Lee, J.; Song, D.; Wang, S. *Dalton Trans.* **2003**, 3493. (d) Wadas, T. J.; Lachicotte, R. J.; Eisenberg, R. *Inorg. Chem.* **2003**, *42*, 3772.

(8) (a) Experimental work: Lu, W.; Mi, B.-X.; Chan, M. C. W.; Hui, Z.; Zhu, N.; Lee, S.-T.; Che, C.-M. *Chem. Commun.* **2002**, 206. (b) DFT and TD-DFT Computations: Zhou, X.; Pan, Q.-J.; Xia, B.-H.; Li, M.-X.; Zhang, H.-X.; Tung, A.-C *J. Phys. Chem. A* **2007**, *111*, 5465.

10.1021/om700997v CCC: $40.75
Publication on Web 03/15/2008

Scheme 1

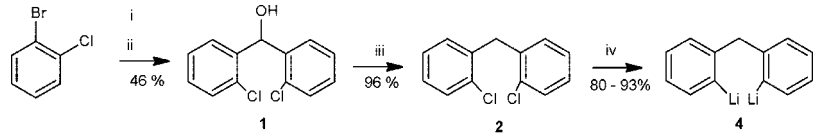

(i) activated Mg turnings, diethyl ether (ii) 2-chlorobenzaldehyde, diethyl ether
(iii) H_3PO_2,AcOH,I_2; (iv) Na-enriched Li (reagent **3**)

Scheme 2

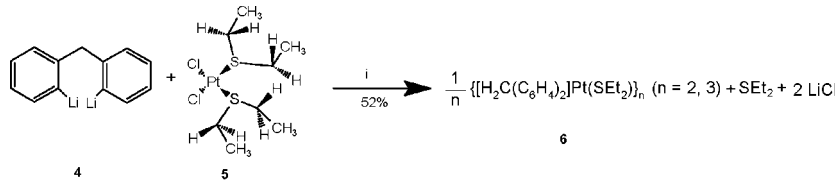

(i) Diethyl ether, room temperature, 4 hrs.

either 1,4-diaza-1,3-butadienes,[9] aromatic diimines[10] (such as 2,2′-bipyridines or 1,10-phenanthrolines), substituted pyridylbenzimidazoles,[11] or substituted dipyridylamines.[12] While this list is not exhaustive, it is interesting that six-membered metallacycles are underutilized, and the promising luminophores that could be obtained with nitrogen-chelated 9,10-dihydroplatinaanthracenes have not been synthesized so far. Platinum-based luminescent materials are of great interest as efficient emitting layers in organic light-emitting diodes (OLEDs).[13] Here, we report the syntheses of the first 9,10-dihydroplatinaanthracenes containing nitrogen-based ligands. Most of the new compounds show intense luminescence, and varying the nitrogen ligand allows facile tuning of the emission frequency from green to red. We are complementing the synthetic and spectroscopic data with electrochemical data and MO computations, in order to gain insight into how changing the ligand affects orbital energies.

Results and Discussion

Syntheses. All luminescent complexes in this work were synthesized using a dialkylsulfide-bridged oligomer, $\{[H_2C(C_6H_4)_2]Pt(SEt_2)\}_n$ ($n = 2, 3$), as the precursor providing the metallacyclic units. The oligomer was prepared in four steps by modification of published procedures, using commercially available compounds (Schemes 1 and 2). The Grignard reagent derived from 1-bromo-2-chlorobenzene was coupled with 2-chlorobenzaldehyde to yield 2,2′-dichlorodiphenylmethanol (Scheme 1, compound **1**). Reduction provided 2,2′-dichlorodiphenylmethane (**2**) in excellent yield. Crucial for the assembly of the metallacyclic unit is the use of lithium containing a very well-defined amount of sodium (2.5%), as suggested by Pringle.[14] Sodium-enriched lithium (**3**) proved essential for the synthesis of 2,2′-dilithiodiphenylmethane (**4**). Compound **4** has to be carefully prepared to control the amount of basic impurities (see Experimental Section), which then allows smooth reaction of an ether solution of **4** with cis-$PtCl_2(SEt_2)_2$ (**5**, Scheme 2) to produce metallacyclic **6** (Experimental Section). The oligomer **6** is obtained as a mixture of a major (78%, per Pt) and a minor (22%) species, which both have the composition "$[H_2C(C_6H_4)_2]Pt(SEt_2)$" and appear to differ only by the degree of oligomerization (cyclic dimer vs. cyclic trimer). From a synthetic point of view, the mixture is an excellent reagent for the synthon "$[H_2C(C_6H_4)_2]Pt$". Adding an excess of free diethyl sulfide quantitatively yields a mononuclear complex containing two SEt_2 molecules per Pt, namely, $[H_2C(C_6H_4)_2]Pt(SEt_2)$, **6b**. We note that **6**, $\{[H_2C(C_6H_4)_2]Pt(SEt_2)\}_n$ ($n = 2, 3$), is reasonably stable to air and water, and it appears as an off-white solid that is sparingly soluble in most organic solvents. ^{1}H NMR spectroscopy demonstrates for **6** that the two methylene hydrogens (exhibiting platinum satellites) are chemically inequivalent, as previously observed[4] for the phosphine-ligated platinum(II) complexes. A very similar observation is made for **6b**, $[H_2C(C_6H_4)_2]Pt(SEt_2)_2$, shown in Figure 1.

NOESY experiments (at 0 °C in dichloromethane-d_2) confirm that the axial proton (proton spatially closer to the Pt atom) gives rise to the largest platinum coupling for the peak which is located further downfield in the ^{1}H NMR spectrum. Somewhat related close spatial proximities have been reported for a system where a chelating bis(N-7-azaindolyl)methane, having a central CH_2 moiety, was used.[15] It was reported that the seven-membered ring was severely puckered and that the CH_2 moiety was rather close to Pt, with the shorter Pt−H distance being 2.44 Å from the platinum center. For the compounds we report here, the six-membered ring of the $[H_2C(C_6H_4)_2]Pt$ unit should provide for a larger Pt−H distance, and in fact we observe for a $[H_2C(C_6H_4)_2]Pt$ unit chelated by 2,9-dimethylphenanthroline (see below) that the closest Pt−H distance involving a metallacyclic methylene hydrogen is 3.07 Å. It is likely that the larger $^4J_{PtH}$ coupling for the proton closer to the platinum center is due to some "through-space" coupling component.

With precursor **6** in hand, synthesis of the nitrogen-chelated complexes proved straightforward. All chelate ligands used were commercially available, with the exception of 4,4′-bis(dimethyl-

(9) (a) Kaim, W.; Klein, A.; Hasenzahl, S.; Stoll, H.; Záliš, S.; Fiedler, J. *Organometallics* **1998**, *17*, 237. (b) Klein, A.; van Slageren, J.; Záliš, S. *Inorg. Chem.* **2002**, *41*, 5216.

(10) (a) Klein, A.; Kaim, W. *Organometallics* **1995**, *14*, 1176. (b) Dungey, K. E.; Thompson, B. D.; Kane-Maguire, N. A. P.; Wright, L. L. *Inorg. Chem.* **2000**, *39*, 5192. (c) Klein, A.; van Slageren, J.; Záliš, S. *Eur. J. Inorg. Chem.* **2003**, 1917.

(11) Liu, Q.-D.; Jia, W.-L.; Wang, S. *Inorg. Chem.* **2005**, *44*, 1332.

(12) Liu, Q.-D.; Jia, W.-L.; Gang, W.; Wang, S. *Organometallics* **2003**, *22*, 3781.

(13) (a) Baldo, M. A.; O'Brien, D. F.; You, Y.; Shoustikov, A.; Sibley, S.; Thompson, M. E.; Forrest, S. R. *Nature* **1998**, *395*, 151. (b) Wong, W.-Y.; He, Z.; So, S.-K.; Tong, K.-L.; Lin, Z. *Organometallics* **2005**, *24*, 4079. (c) He, Z.; Wong, W.-Y.; Yu, X.; Kwok, H.-S.; Lin, Z. *Inorg. Chem.* **2006**, *45*, 10922. (d) Evans, R. C.; Douglas, P.; Winscom, C. J. *Coord. Chem. Rev.* **2006**, *250*, 2093. (e) Zhou, G.-J.; Wang, X.-Z.; Wong, W.-Y.; Yu, X.-M.; Kwok, H.-S.; Lin, Z. *J. Organomet. Chem.* **2007**, *692*, 3461.

(14) Pringle, P. G. (University of Bristol), personal communication.

(15) Song, D.; Wang, S. *Organometallics* **2003**, *22*, 2187.

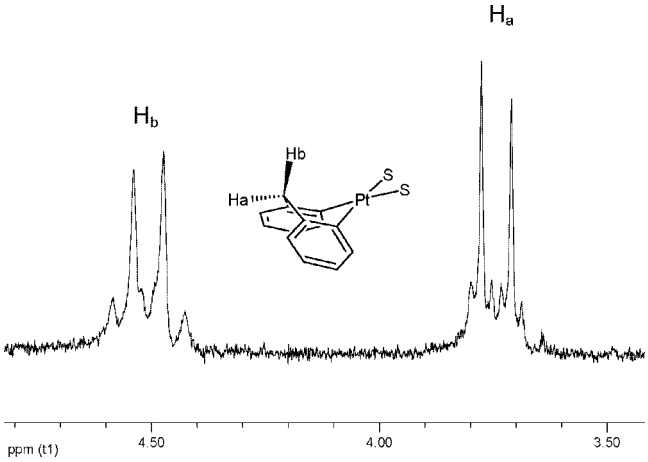

Figure 1. Room-temperature 200 MHz ^{1}H NMR spectrum, in C_6D_6, of the methylene region of **6b**, $[H_2C(C_6H_4)_2]Pt(SEt_2)_2$, obtained from cyclic oligomer **6** using an excess of SEt_2. Peaks appear at 3.74 ($1H_a$, d, C−H, $^4J_{PtH}$ = 9.6 Hz, J_{HH} = 13.0 Hz) and 4.51 ($1H_b$, d, C−H, $^4J_{PtH}$ = 18.8 Hz, J_{HH} = 13.2 Hz). Assignment was confirmed by NOESY (Experimental Section).

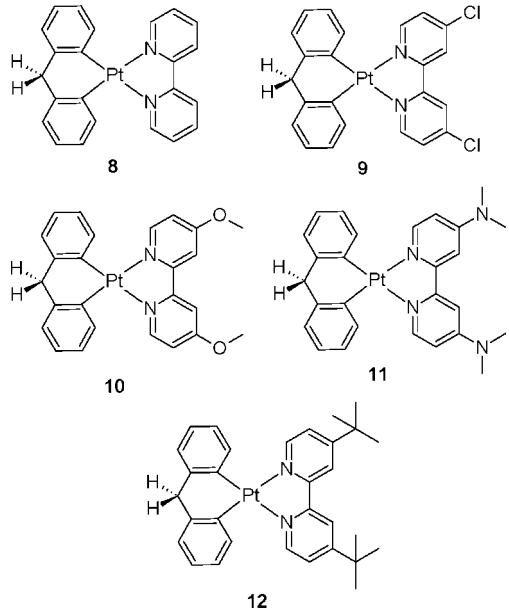

Figure 2. 2,2′-Bipyridine series: compounds **8**–**12**.

amino)-2,2′-bipyridine (**7**), which was prepared according to a modified literature procedure (see Experimental Section). Synthesis of the monomeric nitrogen-chelated metallacyclic compounds **8**–**17** was achieved by adding 1 equiv of the nitrogen donor ligand per one Pt of **6**, followed by gentle reflux in benzene. The bipyridine-derived compounds (**8**−**12**) are shown in Figure 2, whereas the phenanthroline-derived compounds (**13**−**15**) are shown in Figure 3. The compounds derived from 2,2′-biquinoline (**16**) and *N,N,N′,N′*-tetramethylethylenediamine (tmeda) (**17**) are shown in Figure 4. All new nitrogen chelates **8**−**17** were unambiguously characterized, including elemental analysis, as described in the Experimental Section. For the majority of complexes, both ^{1}H and ^{13}C NMR spectroscopic data were obtained. For the few examples where solubility was very low, only ^{1}H NMR spectroscopy was performed, and it was then performed at elevated temperature. UV–visible spectroscopy was performed on all compounds **8**–**17**, discussed in detail below. The metallacyclic compounds are air- and water-stable as solids, but mildly hygroscopic. The important NMR

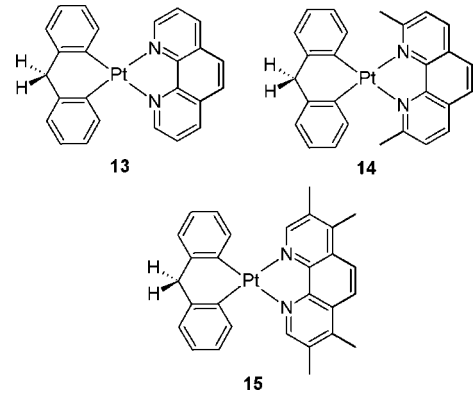

Figure 3. 1,10-Phenanthroline series: compounds **13**–**15**.

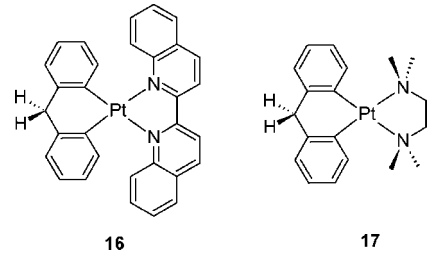

Figure 4. Compounds derived from 2,2′-biquinoline (**16**) and tmeda (**17**).

spectroscopic observation is made that the two methylene protons on every metallacyclic compound (**8**–**17**) are not equivalent, such that the relative rigidity, on the time scale given by the magnetic field strength and the peak-to-peak separation, that was seen for **6** and **6b** (see above) is also present in the luminescent materials **8**−**16** and compound **17**. Also, Pt satellites are clearly seen for each of the two methylene protons (best observed at low field strength).

Structure of $[H_2C(C_6H_4)_2]$Pt(2,9-dimethyl-1,10-phenanthroline) (14). Crystals suitable for X-ray diffraction were obtained for $(CH_2(C_6H_4)_2)$Pt(2,9-dimethyl-1,10-phenanthroline), compound **14**. A single-crystal X-ray structure determination (details in the Experimental Section, molecular structure in Figure 5) confirmed that the desired product has been made and provides relevant data on the geometry of the nitrogen ligand and the metallacyclic moiety.

The platinum environment can be described as approximately square-planar, but distortions from planarity, likely caused by steric repulsion (methyl groups on the phenanthroline ligand), are significant: Pt1 is dislocated by 0.1023(3) Å from the plane formed by the donor atoms (N1, N1′, C1, C1′). The platinacycle adopts a very pronounced boat conformation (see Figure 5), similar to the boat conformation of $[H_2C(C_6H_4)_2]Pt(PEt_3)_2$.[4,16] The 2,9-dimethyl-1,10-phenanthroline ligand is not planar, and best planes through the outer aromatic rings of this nitrogen ligand form a dihedral angle of 18.9(3)°. The phenanthroline ligand plane (defined by N1, C13, C13′, N1′) forms a dihedral angle of 30.8(3)° with the PtN_2 plane (Pt1, N1, N1′), demonstrating the pucker in the five-membered chelate ring involving the nitrogen ligand. It is relevant here that π-stacking interactions and Pt−Pt close contacts can occur in solid-state structures of platinum compounds, and it is known that such interactions can influence the emissive properties of platinum(II) luminophores.

(16) DFT computations using RB3LYP and the SDD basis set also predict a boat-shape conformation of all platinacycles. Compound **13** is shown in the Supporting Information.

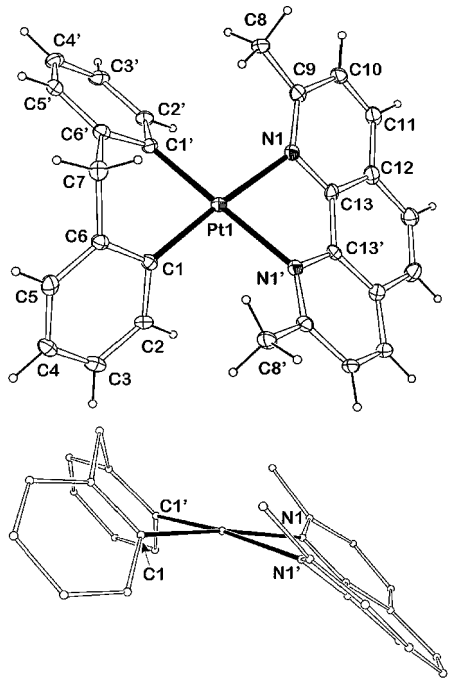

Figure 5. Molecular structure of $[H_2C(C_6H_4)_2]$Pt(2,9-dimethyl-1,10-phenanthroline) (**14**). In addition to a thermal ellipsoid plot (top, 30% probability; hydrogens as spheres of arbitrary radius), a ball-and-stick plot (bottom, hydrogens omitted for clarity) is shown in order to highlight the geometry of the six-membered chelate ring. The molecule has crystallographic mirror symmetry (mirror plane through C7, Pt1, and the center between N1 and N1′). Selected distances and angles (Å, deg): Pt1−C1, 1.999(5); Pt1−N1, 2.130(5); C1−Pt1−C1′, 83.9(3); N1−Pt1−N1′, 78.1(2); C1−Pt1−N1′, 98.7(2); C1−Pt1−N1, 173.6(2); arenes in the metallacyclic ring are not coplanar: dihedral angle between best plane through C1−C2−C3−C4−C5−C6 and best plane through C1′−C2′−C3′−C4′−C5′−C6′, 67.6(3); boat conformation of the metallacyclic ring: dihedral angle between plane through C1−Pt1−C1′ and plane through C6−C7−C6′, 86.0(6).

In a study by Lu et al.,[17] where such effects were seen, $\pi-\pi$ contacts were crystallography determined to be in the 3.12 to 3.40 Å range. Pt−Pt distances in complexes where the Pt−Pt interaction has a significant impact on luminescent properties are typically around 3.5 Å.[18] In the crystal structure of compound **14**, however, the closest Pt−Pt distance is 5.331(3) Å, the closest ring centroid separation is 4.577(3) Å, and this is outside the range for significant $\pi-\pi$ stacking interactions. No close, parallel packing of π-ligands is observed in the solid-state structure. Apparently, the pronounced pucker of the six-membered metallacyclic ring prevents packing involving significant π-stacking. A similar puckered structure also exists for the remaining compounds, as judged from the fact that all compounds show nonequivalent methylene hydrogens in the ^{1}H NMR spectrum. All emissions are in the visible range, and visually, emissions have the same color for microcrystalline powder and frozen, glassy, dilute solutions (benzene, dimethylsulfoxide, tetrahydrofuran, dichloromethane, and hexanes), demonstrating that the emissive properties are due to electronic effects within the molecule and are not significantly influenced by stacking effects.

UV/Vis Absorption. UV–vis spectra were obtained for compounds **8** to **17**, and the data are summarized in Table 1. The lowest-energy bands (in acetonitrile) for the 2,2′-bipyridine series, the 1,10-phenanthroline series, and the set having the two remaining compounds (biquinoline and tmeda) are shown in Figures 6, 7, and 8, respectively (see Supporting Information for complete UV–vis spectra). The position of the lowest-energy absorption maximum strongly depends on the nature of the nitrogen chelate. For compounds containing substituted 2,2′-bipyridines (**8**–**12**, Figure 6) and 1,10-phenanthrolines (**13**–**15**, Figure 7), the positions of the maxima are in the range between 395 and 455 nm, where the 395 nm value refers to the highly electron-rich 4,4′-bis(dimethylamino)-2,2′-bipyridine complex **11** and the 455 nm value to the electron-deficient 4,4′-dichloro-2,2′-bipyridine complex **9**. This dependence suggests that the lowest-energy transition is a transition from an orbital that is largely unaffected by substituents on the nitrogen chelate (likely located on the metallacyclic ring and/or Pt) into an empty π^* orbital on the nitrogen chelate, a situation that is frequently encountered when the Pt(II) is in a strong-field environment, such as provided by two aryls. DFT computations (below) will show that these excitations indeed occur from an orbital that is located at the metallacycle and Pt (the HOMO or an energetically very close filled orbital) into normally the LUMO, which is essentially a purely diimine-based π^* orbital. Such transitions would be called "ligand-to-ligand charge transfer" (LLCT, from metallacyclic ligand to diimine) if the fact is ignored that the donor orbital has a small but not completely negligible coefficient involving a platinum d orbital. However, since the donor orbital has mixed ligand/metal character, a more accurate term is "mixed-metal/ligand-to-ligand" charge transfer (MMLLCT).[7] Similar MMLLCT transitions have been reported for the five-ring metallacycle systems Pt(biphenyl-diyl)(diimine).[19] The slightly more general term "charge-transfer-to-diimine" is equally applicable. Expectedly, the lowest-energy transition[20] occurs at very high energy (281 nm) when a π-system on the nitrogen chelate is missing, such as in **17**, and occurs at very low energy for an extended π-system, such as in **16**, at 523 nm.

Compound **16** has an extended π-system which shows a four-band structure spectrum. We tentatively assign the 250 nm peak to a π to π^* intraligand transition (ILT) of the C^C part of the molecule, while a broadened peak in the 280–380 nm region may be attributed to a π to π^* intraligand transition (ILT) of the extended N^N part of the molecule. The lowest-energy transition occurs at 523nm, assigned as a charge-transfer-to-diimine.

Electrochemistry. Cyclic voltammetry was used to determine the ground-state redox potentials for complexes **8**−**17**. The redox potentials, where reversibility or lack thereof is indicated, are included in Table 1. Typically, the complexes each display two diimine-based reduction potentials (no reduction for the tmeda-chelated complex **17**) and, possibly due to the restrictions imposed by solvent oxidation at very positive potentials, only one oxidation potential. The first reduction process is for the most part reversible, while the second one is mostly quasi-reversible or irreversible. The oxidation waves are irreversible (even fast sweep rates and small solvent windows) with the exception of the tmeda complex **17**, which exhibits a quasi-reversible wave. This might be due to steric stabilization of the Pt(III) intermediate, via the added steric bulk.[21] The reduction

(17) Lu, M.; Chan, M. C. W.; Cheung, K.-K.; Che, C.-M. *Organometallics* **2001**, *20*, 2477.

(18) Miskowski, V. M.; Houlding, V. H.; Che, C.-M.; Wang, Y. *Inorg. Chem.* **1993**, *32*, 2518.

(19) Blanton, C. B.; Murtaza, Z.; Shaver, R. J.; Rillema, D. P. *Inorg. Chem.* **1992**, *31*, 3230.

(20) For a discussion of what will be the lowest-energy transition in which metal complex: Roundhill, D. M. *Photochemistry and Photophysics of Metal Complexes*; Plenum Press: New York, 1994; p 81.

Table 1. Absorption Spectral and Electrochemical Data for Compounds 8 to 17 at Room Temperature

complex	λ_{abs}/nm (ϵ/10^4 M^{-1} cm^{-1})[a]	$E_{1/2}^{ox}$/V (vs Fc^+/Fc)[a]	$E_{1/2}^{red}$/V (vs Fc^+/Fc)[a]
$Pt(CH_2(C_6H_4)_2)$(2,2′-bipyridine), **8**	188 (2.98), 207 (2.64), 240sh (0.930), 290 (0.709), 429 (0.190)	0.612[d]	−1.91, −2.57[c]
$Pt(CH_2(C_6H_4)_2)$(4,4′-dichloro-2,2′-bipyridine), **9**	192 (3.98), 203 (4.10), 249sh (0.641), 296 (0.512), 455 (0.130)	0.671[d]	−1.66, −2.33[d,e]
$Pt(CH_2(C_6H_4)_2)$(4,4′-dimethoxy-2,2′-bipyridine), **10**	199 (17.22), 210 (17.76), 231sh (7.43), 275 (4.54), 289sh (3.63), 411 (0.721)	0.551[d]	−2.02[c], −2.69[c]
$Pt(CH_2(C_6H_4)_2)$(4,4′-bis(dimethylamino)-2,2′-bipyridine), **11**	191 (6.06), 207 (7.44), 268 (4.76), 294sh (2.86), 309sh (2.57), 395 (0.80)	0.42[b,d,e]	−2.33[b,c] −3.05[b,d]
$Pt(CH_2(C_6H_4)_2)$(4,4′-di-*tert*-butyl)-2,2′-bipyridine), **12**	192 (5.22), 203 (5.39), 246sh (1.09), 296 (1.10), 421 (0.265)	0.597[d]	−2.01, −2.64[c]
$Pt(CH_2(C_6H_4)_2)$(1,10-phenanthroline), **13**	192 (4.97), 203 (5.71), 225sh (1.85), 267 (1.17), 296sh (0.39), 347sh (0.102), 379sh (0.12), 430 (0.17)	0.53[d,e]	−1.93, −2.55[c,e]
$Pt(CH_2(C_6H_4)_2)$(2,9-dimethyl-1,10-phenanthroline), **14**	192 (4.42), 203 (4.54), 232 (2.88), 271 (1.65), 293sh (0.988), 361 (0.23), 423 (0.23)	0.648[d]	−2.09[c], −2.81[c,e]
$Pt(CH_2(C_6H_4)_2)$(3,4,7,8-tetramethyl-1,10-phenanthroline), **15**	192 (5.51)[f], 210 (6.76)[f], 231sh (3.89)[f], 272 (3.53)[f], 306sh (1.39)[f], 405 (0.55)[f]	0.45[d,e] 0.59[b,d,e]	−2.21[c], −2.91[c] −2.10[b,c], −2.48[b,c]
$Pt(CH_2(C_6H_4)_2)$(2,2′-biquinoline), **16**	191sh (2.97), 207 (3.51), 259 (2.51), 275sh (1.37), 309sh (0.81), 328 (0.79), 340sh (0.68), 374 (0.17), 523 (0.07)	0.785[d]	−2.05[c], −2.40[d,e]
$Pt(CH_2(C_6H_4)_2)$(*N,N,N′N′*-tetramethylethylenediamine), **17**	194 (9.08), 209sh (7.67), 265 (1.33), 281 (1.31), 287sh (1.18)	0.513[c]	no reductions visible

[a] UV–vis spectra and electrochemical data were measured in anhydrous deoxygenated CH_3CN using a quartz cuvette unless otherwise noted. [b] Electrochemical measurement was performed in anhydrous, degassed DMF. [c] Quasireversible process. [d] Irreversible process. [e] Broad. [f] Larger error associated in the determination of ϵ (up to ±30%) due to very low solubility. See Supporting Information for UV/vis spectra and CV diagrams.

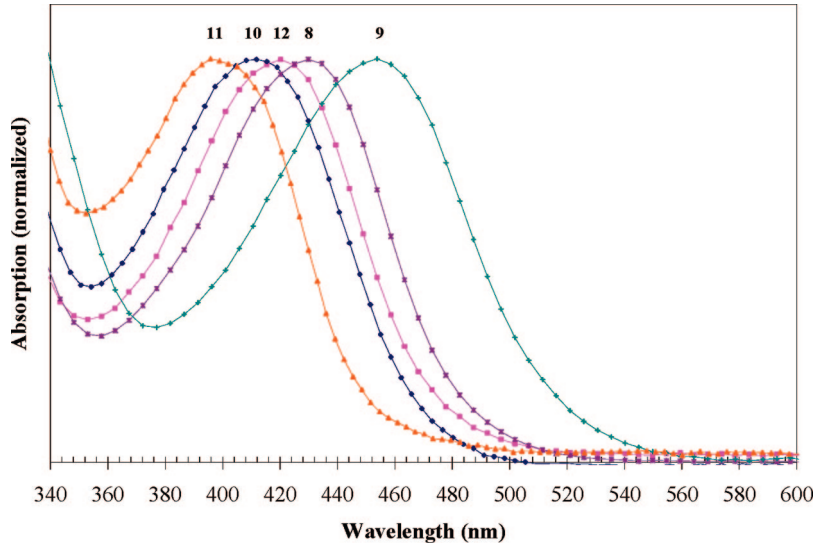

Figure 6. Charge-transfer-to-diimine absorption bands (normalized, in acetonitrile at room temperature) for 2,2′-bipyridine-derived Pt-metallacycle series, having the following ligands: 2,2′-bipyridine (for **8**), 4,4′-dichloro-2,2′-bipyridine (for **9**), 4,4′-dimethoxy-2,2′-bipyridine (for **10**), 4,4′-bis(dimethylamino)-2,2′-bipyridine (for **11**), 4,4′-di-*tert*-butyl-2,2′-bipyridine (for **12**).

values correlate well with the donating ability of the N^N chelate. The more donating the ligand is, the more negative the first reduction potential becomes. For the electron-rich compound **11**, chelated by 4,4′-bis(dimethylamino)-2,2′-bipyridine, the first (reversible) reduction occurs at −2.33 V, whereas the system involving the least electron-rich ligand, namely, compound **9** (having 4,4′-dichloro-2,2′-bipyridine), is reduced at −1.66 V. The order of decreasing ease of reduction follows **9**, **8**, **12**, **10**, and **11** for the 2,2′-bipyridine series and **13**, **14**, and **15** for the 1,10-phenanthroline series. A representative example is shown in Figure 9, the cyclic voltammogram (CV) of 4,4′-di-*tert*-butyl-2,2′-bipyridine, **12**. One reversible reduction occurs at −2.01 V, a quasi-reversible reduction occurs at −2.64 V, and an irreversible oxidation occurs at 0.597 V relative to the internal ferrocene/ferrocenium (Fc/Fc^+) reference couple.

The substituted 1,10-phenanthroline series shows a similar trend, with the most electron-rich diimine, 3,4,7,8-tetramethyl-1,10-phenanthroline, giving rise to the most negative first reduction potential, namely, −2.21 V, whereas −1.93 V is observed for the system having the less electron-rich ligand 1,10-phenanthroline. Correlations between electrochemical and spectroscopic data are well-known.[22–24] In the particular case of a charge-transfer-to-diimine as the lowest-energy optical transition, the transition can be viewed as ejection of an electron out of one of the highest occupied molecular orbitals (metallacycle-Pt based, orbital energy probed by the redox potential for oxidation) and injection of an electron into the diimine-based LUMO (orbital energy probed by the first reduction potential). The correlation is very good for the new metallacyclic systems, and Figure 10 shows a plot of the photon energy for absorption versus "empirical HOMO–LUMO gap", as defined by the difference between potential for first oxidation and potential for first reduction. The data show a good linear agreement, and a small intercept (0.41) combined with a slope of very close to

(21) Johansson, L.; Ryan, O. B.; Rømming, C.; Tilset, M. *Organometallics* **1998**, *17*, 3957.
(22) Cummings, S. D.; Eisenberg, R. *J. Am. Chem. Soc.* **1996**, *118*, 1949.
(23) Lever, A. B. P.; Pickens, S. R.; Minor, P. C.; Licoccia, S.; Ramaswamy, B. S.; Magnell, K. *J. Am. Chem. Soc.* **1981**, *103*, 6800.
(24) Rezvani, A. R.; Crutchley, R. *Inorg. Chem.* **1994**, *33*, 170.

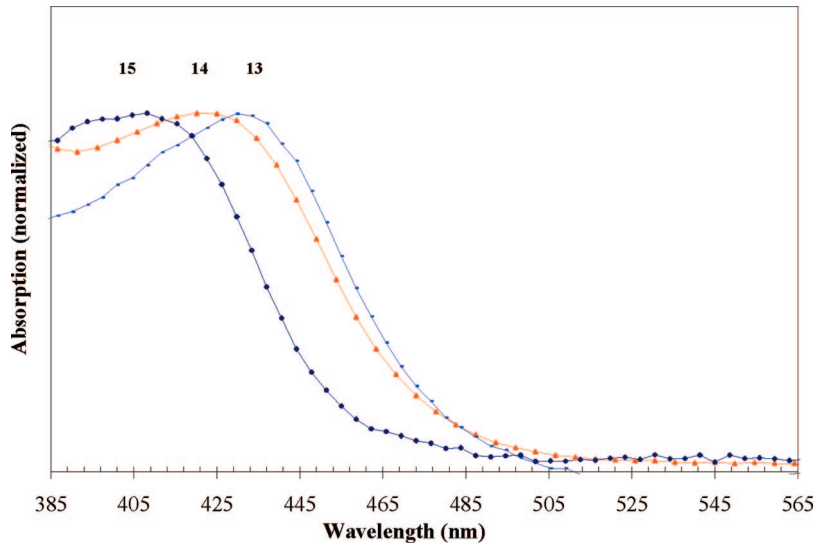

Figure 7. Charge-transfer-to-diimine absorption bands (normalized, in acetonitrile at room temperature) for 1,10-phenanthroline-derived Pt-metallacycle series, using the following ligands: 1,10-phenanthroline (for **13**), 2,9-dimethyl-1,10-phenanthroline (for **14**), 3,4,7,8-tetramethyl-1,10-phenanthroline (for **15**).

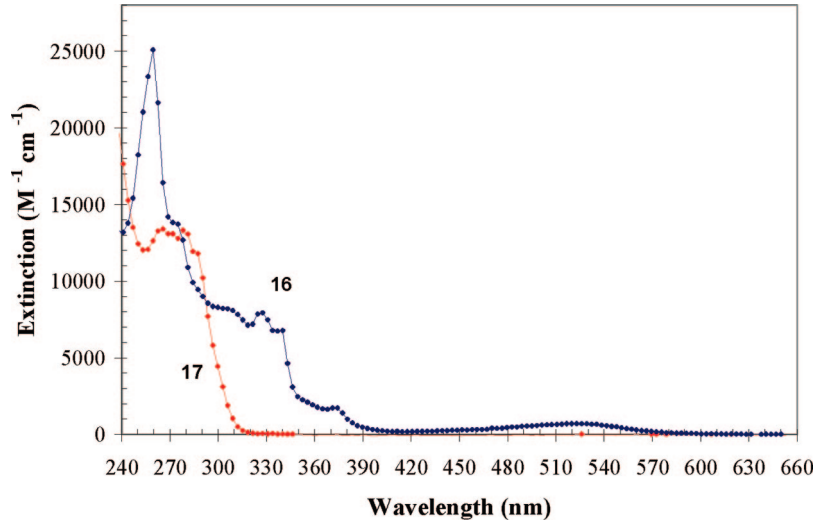

Figure 8. UV–vis spectra showing molar absorptivities for the complexes of 2,2′-biquinoline (for **16**) and *N*,*N*,*N*′*N*′-tetramethylethylenediamine (for **17**), in acetonitrile at room temperature.

unity (0.99) demonstrates that the "empirical HOMO–LUMO gap", as measured by electrochemistry, is indeed a very reasonable predictor of the lowest-energy optical absorbance. Computations are complementing our experimental data, and we will discuss computed (DFT) HOMO–LUMO gaps below. It can be mentioned here that a good correlation also exists for the DFT-calculated HOMO–LUMO gap vs the difference between the ground-state oxidation and reduction potentials (see Supporting Information for plot).

Luminescence. When excited with UV light (365 nm), all solid, microcrystalline samples of compounds **8**−**16**, that is, all nitrogen-chelated Pt compounds described here except the tmeda-chelated **17**, show bright emission at room temperature, ranging from green, yellow, orange to red. Pictures of luminescent powders are shown in Figure 11, emission spectra for **8**−**12** are shown in Figure 12, and peaks are tabulated in Table 2. Very similar emissions are obtained from frozen solutions at liquid nitrogen temperature, but no emission is detected at room temperature in benzene, hexanes, dimethylsulfoxide, tetrahydrofuran, and dichloromethane solution (concentration ~0.0001 M). Interaction with solvent or self-quenching[25] might be responsible for the apparent lack of emission in room-temperature solution, which contrasts with intense emission from the solid state. In our quest to tune the emission wavelengths such that a large part of the visible spectrum is covered, we found that the emission wavelength is straightforwardly influenced for the substituted 2,2′-bipyridine series. With the exception of 4,4′-bis(dimethylamino)-2,2′-bipyridine (**11**), the more donating the ligand is, the higher the energy of emission becomes, where 4,4′-dimethoxy-2,2′-bipyridine (**10**) as a ligand effects a broad emission in the green region, at 536 nm. The most electron-deficient substituted 2,2′-bipyridine, 4,4′-dichloro-2,2′-bipyridine (**9**), lead to a red-shifted emission in the orange region, at 595 nm (Figure 12).

However, no such clear trend is visible for the emission maxima belonging to the small series (three members) containing 1,10-phenanthroline (structures in Figure 3, emission spectra in the

(25) (a) Connick, W. B.; Geiger, D.; Eisenberg, R. *Inorg. Chem.* **1999**, *38*, 3264. (b) Fleeman, W. L.; Connick, W. B. *Comments Inorg Chem.* **2002**, *23*, 205.

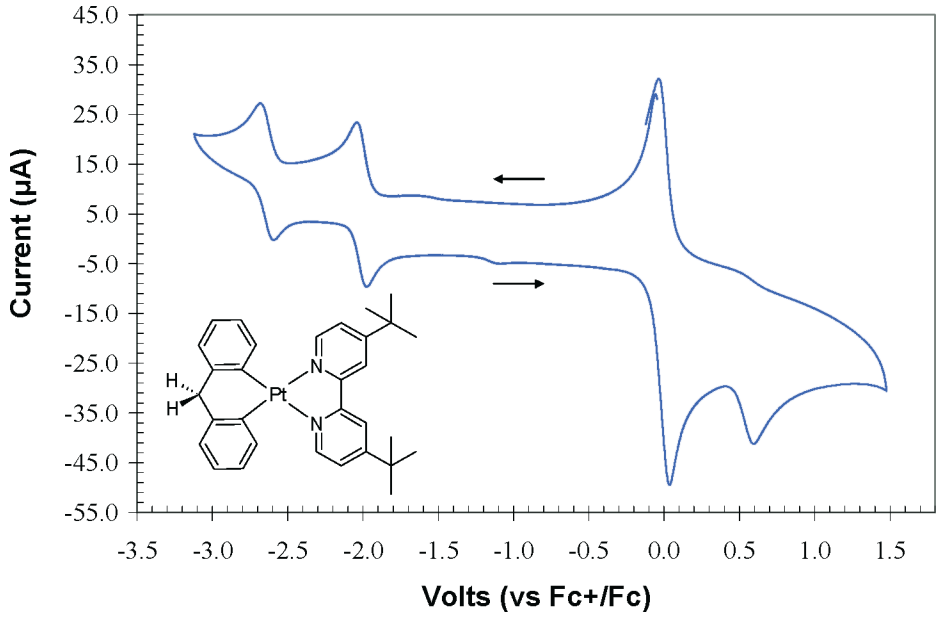

Figure 9. Cyclic voltammogram (CV) of **12**, measured in acetonitrile at 28 °C. Potentials are referenced relative to internal Fc/Fc^{+} (defined as 0 V). Scan rate is 1000 mV/s. TBAHFP (0.1 M) was used as the supporting electrolyte.

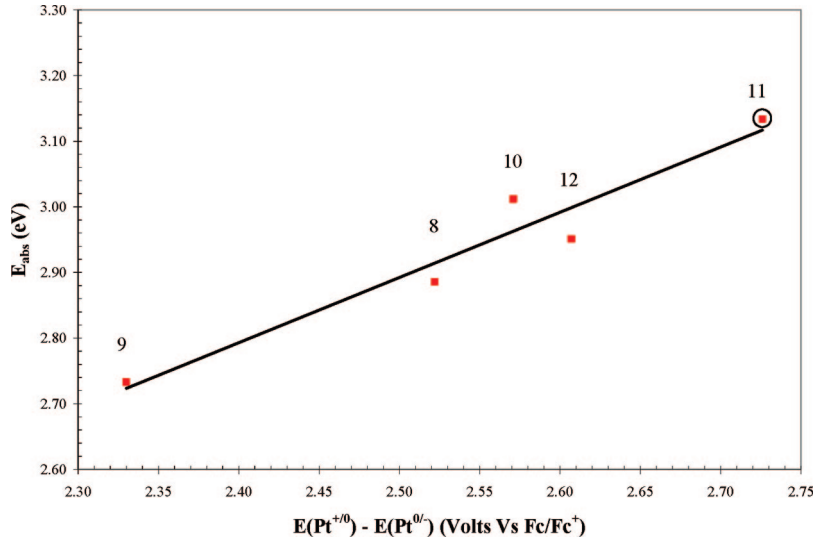

Figure 10. Plot of experimental (UV–vis, acetonitrile) transition energy for absorbance, E_{abs}, vs the difference between the ground-state oxidation and reduction potentials, for complexes **8** to **12**. Linear regression analysis yields $R^2 = 0.9338$, and equation of line is $y = 0.9929x + 0.41$. Circled datum denotes electrochemical data obtained in DMF solvent.

Supporting Information), and this might be related to the broad and complex nature of the emission bands for the 1,10-phenanthroline-derived compounds. Furthermore, the 2,2′-biquinoline complex **16** yields deep red luminescence at 690 nm, whereas the tmeda complex **17** yields no significant emission.

DFT Calculations. Molecular orbital calculations (Gaussian 03) using Becke's hybrid three-parameter functional with Lee, Yang, and Parr correlation functional (B3LYP),[26,27] a variant of density functional theory (DFT), were performed on the ground states (singlet) of the new diimine compounds **8**−**16** and the tmeda compound **17**, in order to determine the energies of the high-lying filled and the low-lying unoccupied orbitals and to test the hypothesis that the former ones are localized largely on the metallacycle and the latter ones, for diimine compounds, largely on the diimine. As can be seen from Figures 13,14,15, for all compounds (see Supporting Information as well), the HOMO is mainly metallacycle-based with some d-orbital contribution from Pt. For all diimine-based compounds, the LUMO is almost entirely based on the diimine ligand. Consequently, substituents on the diimine influence the HOMO very little but have a pronounced effect on the LUMO. It results that the HOMO–LUMO gap is strongly influenced by substituents on the diimine, and the HOMO–LUMO gaps range from as low as 53.34 kcal/mol to as high as 62.75 kcal/mol. This 9.41 kcal/mol range (gas phase) is responsible for the fact that the position of the low-energy absorbance maximum is easily tuned by attaching electron-donating or electron-withdrawing substituents to the metallacycle. Similarly, the emission properties are tuned. While the emission maxima are, naturally, shifted to higher wavelength compared to the charge-transfer-to-diimine absorbances (data in Table 2), a change in the electron density

(26) Becke, A. D. *J. Chem. Phys.* **1993**, *98*, 5648.
(27) Stephens, P. J.; Devlin, F. J.; Cabalowski, C. F.; Frisch, M. J. *J. Phys. Chem.* **1994**, *98*, 11623.

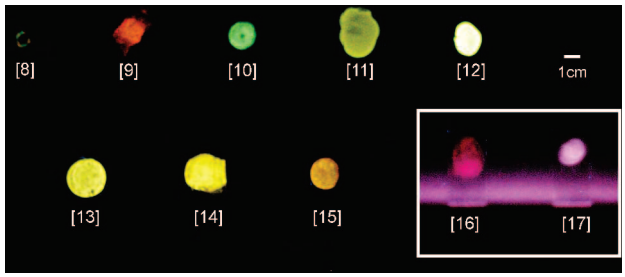

Figure 11. Room-temperature luminescence, caused by 365 nm excitation, from powder samples (thin layer) of compounds **8**−**17**. Regarding apparent relative intensities: layer thickness was not uniform and the brightness/contrast of the relatively weakly emitting (very thin layer) sample **8** was enhanced relative to **9**−**15**. Blue specks due to luminescence of the edges of the supporting glass slides were removed from the picture. The photograph of samples **16** and **17**, shown in the inset, was taken with the UV lamp very close (violet strip caused by excitation light).

of the diimine influences the wavelength of the emission in a similar way to how it influences the wavelength of the lowest-energy absorbance. The tmeda complex **17** is computed to have a larger HOMO–LUMO gap of 107.93 kcal/mol, consistent with the experimental observation that it has no charge transfer in the visible region. According to molecular orbital diagrams, the LUMO is diamine-based for complex **17**. In the absence of a π-system on tmeda, the LUMO is based on the saturated backbone and has essentially C−H σ^* character (Supporting Information). In solution phase, using the PCM model (see TD-DFT section, below), the trends are the same, but the HOMO–LUMO gaps are larger (Table 3).

Time-Dependent Density Functional Theory (TD-DFT). Time-dependent density functional theory (TD-DFT) computations were performed in order to more thoroughly probe the nature of the lowest-energy excitations. The most appealing characteristic of TD-DFT is the ability of the computation to predict λ_{max}, which corresponds to vertical electronic transitions computed on the ground-state geometries, especially when solvent effects are accounted for.[28] Solvent effects (solvatochromic shifts) have been previously discussed, using MO calculations, for platinum diimine dithiolate systems that show similar MMLLCT transitions.[29] We performed the computations on the diimine-containing compounds **8** to **16**[30] using RB3LYP with the SDD basis set and acetonitrile solvent (see Experimental Section). It is predicted that the lowest-energy transitions do occur mostly from HOMO−2, HOMO−1, and HOMO to the π^* LUMO of the diimine ligand with the exception of compound **11**, where the MMLLCT is mainly centered in the HOMO–LUMO. Table 4 summarizes the computed three lowest-energy optical transitions for the highly colored diimine-containing compounds **8** to **16**.

The polarizible continuum model (PCM), which we used, is one of the most widely used methods for modeling solvent effects on electronic structure.[31] Despite the fact that the TD-DFT calculations were carried out using PCM, there is still only semiquantitative agreement between the calculated and the observed lowest-energy absorbance maxima. The trends observed are reproduced well by the computations, but the transition energies for the charge-transfer-to-diimine are consistently underestimated by between 9 and 70 nm. This level of disagreement between TD-DFT calculations and experiments is commonly observed, and the extent of disagreement may depend on the strength of the solvatochromism of the molecule.[9b] Factors that likely account for the less-than-perfect agreement between TD-DFT predictions and experimental data are probably relativistic effects (only partially included in the effective core potentials used) and spin–orbit coupling,[31] as well as solute–solvent interactions that go beyond purely electrostatic interactions.

Summary and Conclusion

In summary, the first nitrogen-chelated 9,10-dihydroplatinaanthracenes have been reported, and interesting optical properties are displayed by those compounds that contain aromatic diimine ligands. The lowest-energy optical absorbances are assigned as charge-transfer-to-diimine transitions, as confirmed by DFT and TD-DFT computations. The absorbance maxima are straightforwardly tuned, particularly for the bipyridine-derived systems, using electron-deficient or electron-donating substituents on the diimine, consistent with the proposed nature of these transitions (electron-deficient diimines lead to lower-energy transitions). The diimine-derived systems are strongly luminescent in the solid state at room temperature, and for the most part, different substituents on the diimine shift the emission maxima in the same direction in which they shift absorbance maxima. We have realized emission colors ranging from red to green, and an even wider range can probably be realized. For future applications it may become significant that the arenes in the puckered metallacyclic ring are unable to rotate freely or to easily convert into a planar geometry. It may become important, regarding luminescence quenching mechanisms, that rotation of the arenes is hindered. Also, the "fixed" nonzero angle between the metallacyclic arenes and the diimine unit most certainly makes electronic transitions different from those observed in completely planar systems. Investigations into the details of these effects (such as emission lifetimes) will be the topic of further studies in our group.

Experimental Section

General Information. All manipulations involving organometallic compounds were carried out with the use of a vacuum line and a dry glovebox using oven-dried glassware and J. Young NMR tubes. ^{1}H and ^{13}C{^{1}H} NMR spectra were obtained on Varian Gemini 200 MHz or Unity/Inova Varian 500 MHz spectrometers. All NMR spectra were taken at 20 °C unless otherwise noted. Residual proton and carbon peaks were used as reference: ^{1}H (δ, ppm, chloroform-*d*, 7.24; dichloromethane-d_2, 5.32, benzene-d_6, 7.16, dimethylsulfoxide-d_6, 2.49), ^{13}C (δ, ppm, chloroform-*d*, 77.3; dimethylsulfoxide-d_6, 39.49; dichloromethane-d_2, 53.8). The chemical shifts are reported in parts per million (δ), and the multiplicities are reported as s (singlet), d (doublet), (triplet), q (quartet), m (multiplet), and br (broad). CD_2Cl_2 and $CDCl_3$ were obtained from Cambridge Isotopes and were dried over CaH_2 and vacuum-transferred before use. $(CD_3)_2SO$ and C_6D_6, were purchased from

(28) Jacquemin, D.; Perpète, E. A.; Scalmani, G.; Frisch, M. J.; Ciofini, I.; Adamo, C. *Chem. Phys. Lett.* **2006**, *421*, 272.

(29) (a) Paw, W.; Cummings, S. D.; Mansour, M. A.; Connick, W. B.; Geiger, D. K.; Eisenberg, R. *Coord. Chem. Rev.* **1998**, *171*, 125. (b) Zuleta, J. A.; Bevilacqua, J. M.; Proserpio, D. M.; Harvey, P. D.; Eisenberg, R. *Inorg. Chem.* **1992**, *31*, 2396.

(30) For tmeda-based compound **17**, a lowest-energy transition of 277.9 nm is predicted (experimental: 281 nm), where the transition involves not only the LUMO but also the LUMO+1. However, the LUMO+1 is computed to have a *positive* orbital energy, which indicates that the DFT method employed may not be perfectly applicable to systems where the empty orbitals are very high in energy.

(31) Preat, J.; Loos, P.-F.; Assfeld, X.; Jacquemin, D.; Perpète, E. A. *Int. J. Quantum Chem.* **2007**, *107*, 574.

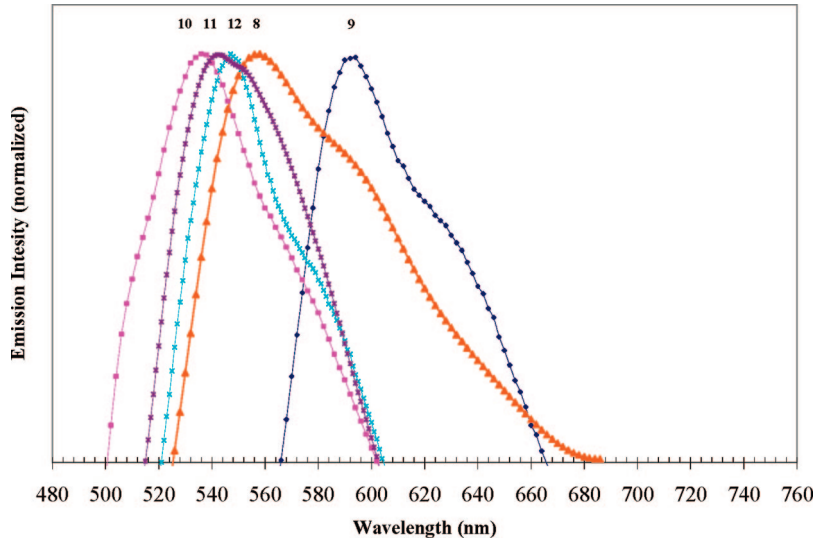

Figure 12. Lowest-energy emission bands for substituted 2,2′-bipyridine series, involving 2,2′-bipyridine (**8**), 4,4′-dichloro-2,2′-bipyridine (**9**), 4,4′-dimethoxy-2,2′-bipyridine (**10**), 4,4′-bis(dimethylamino)-2,2′-bipyridine (**11**), and 4,4′-di-*tert*-butyl-2,2′-bipyridine (**12**), all measured at room temperature in the solid state. Emission intensities have been normalized. $\lambda_{exc} = 425$ nm. Emission spectra for the 1,10-phenanthroline series (**13**−**15**) and 2,2′-biquinoline-derived **16** can be found in the Supporting Information.

Table 2. Room-Temperature, Lowest-Energy Absorption Max in Acetonitrile Solution and Solid Emission Max for Compounds 8 to 17

metallacycle compound	absorption max/nm (nm)[c]	emission max/nm (nm)
2,2′-bipyridine, **8**	429	556[a]
4,4′-dichloro-2,2′-bipyridine, **9**	455	595[a]
4,4′-dimethoxy-2,2′-bipyridine, **10**	411	536[a]
4,4′-bis(dimethylamino)-2,2′-bipyridine, **11**	395	542[a]
4,4′-di-*tert*-butyl-2,2′-bipyridine, **12**	421	548[a]
1,10-phenanthroline, **13**	430	557[a]
2,9-dimethyl-1,10-phenanthroline, **14**	423	565[a]
3,4,7,8-tetramethyl-1,10-phenanthroline, **15**	405	590[a]
2,2′-biquinoline, **16**	523	690[b]
N,N,N′N′-tetramethylethylenediamine, **17**	281	

[a] $\lambda_{exc} = 425$ nm. [b] $\lambda_{exc} = 525$ nm. [c] Measured in acetonitrile solution.

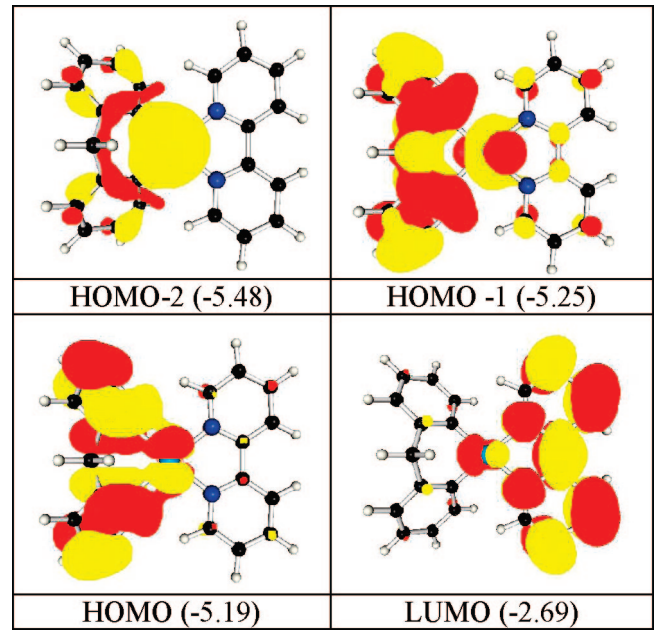

Figure 13. Shapes of relevant orbitals and their energies (eV) for the prototypical 2,2′-bipyridine complex **8**, calculated using G03/RB3LYP using the SDD basis set for singlet ground state (see Supporting Information for compounds **9**–**12**).

Cambridge Isotopes. Diethyl ether, tetrahydrofuran, hexanes, and benzene (protio and deuterated) were dried over sodium-benzophenone and vacuum-transferred before use. Elemental analyses were conducted at Guelph Laboratories, Guelph, ON, Canada, and Analytical Laboratory for Environmental Science and Research Training (ANALEST), Toronto, ON, Canada. Mass spectrometry (MALDI) was conducted at Advanced Instrumentation for Molecular Structure (AIMS), Toronto, ON, Canada.

Chemicals. The diimines, 2,2′-bipyridine (≥99%), 4,4′-di-*tert*-butyl-2,2′-bipyridine (98%), 4,4′-dimethoxy-2,2′-bipyridine (97%), 3,4,7,8-tetramethyl-1,10-phenanthroline (≥99%), 2,9-dimethyl-1,10-phenanthroline (crystalline), 2,2′-biquinoline (98%), and *N,N,N′,N′*-tetramethylethyelenediamine (≥99%) were dried and/or degassed under vacuum (0.006 Torr) and used as received from Aldrich. Anhydrous 1,10-phenanthroline (99%) was purchased from Alfa-Aesar. 4,4′-Dichloro-2,2′-bipyridine (99.9%) was purchased from Carbosynth Limited of the United Kingdom. 4,4′-Bis(dimethylamino)-2,2′-bipyridine was prepared by a modified literature method.[32,33] K_2PtCl_4 (99.9%) was purchased from Strem Chemicals. 2-Bromochlorobenzene (99%), 2-chlorobenzaldehyde (≥99%), Mg, small turnings (99.98%), diethylsulfide (98%), glacial acetic acid (99.7%), iodine chips (99%), hypophosphorous acid (50% aqueous solution), lithium chips (0.5% sodium), 1,2-dibromoethane (≥99%), sodium in kerosene (99%), benzophenone (99%), calcium hydride (≥97%), anhydrous magnesium sulfate (99%), ammonium chloride (≥99.5%), sodium sulfate (≥99.0%), sodium bicarbonate (≥99.5)%, phenolphthalein (pH indicator), and ferrocene (≥98.0%) were purchased from Sigma-Aldrich. 0.02000 N +/−0.00002 hydrochloric acid solution was purchased from VWR International (Ricca Chemicals). Solvents such as anhydrous 1,2,3,4-tetrahydronaphthalene (99%), pentane (99%), acetonitrile (99%), and dimethylformamide (99.8%) were used without any further modification and purchased from Sigma. Electrochemical grade silver nitrate and tetrabutylammoniunhexafluorophosphate (TBAHFP) were also purchased from Sigma. 2,2′-Dichlorodiphenylmethanol was prepared from the following literature method.[34]

(32) Heindel, N. D.; Kennewell, P. D. *J. Chem. Soc. D., Chem. Commun.* **1969**, 38.
(33) Wehman, P.; Dol, G. C.; Moorman, E. R.; Kamer, P. C. J.; van Leeuwen, P. W. N. M.; Fraanje, J.; Goubitz, K. *Organometallics* **1994**, *13*, 4856.

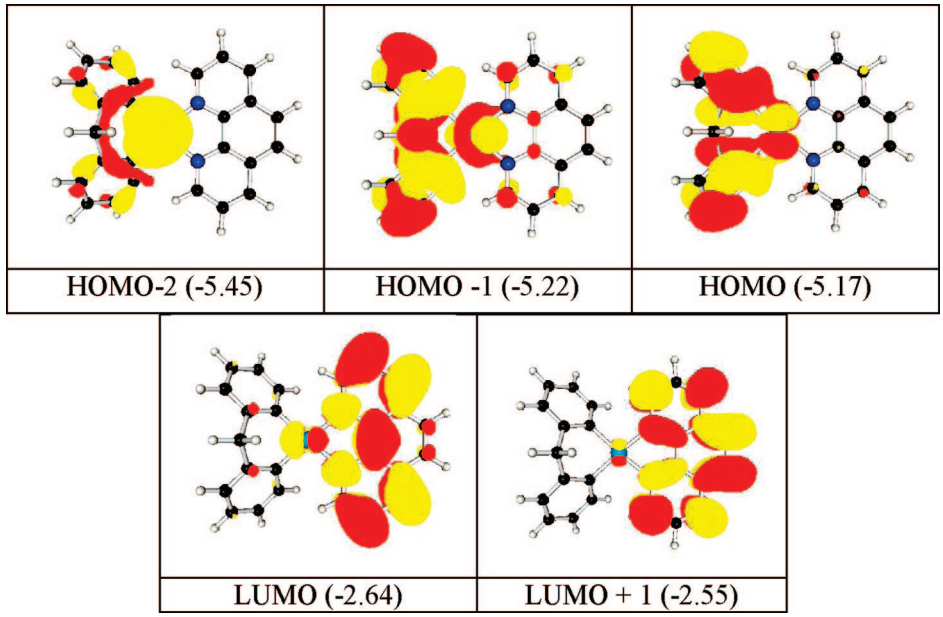

Figure 14. Shapes of relevant orbitals and their energies (eV) for the prototypical 1,10-phenanthroline complex **13**, calculated using G03/RB3LYP using the SDD basis set for singlet ground state (see Supporting Information for compounds **14** and **15**).

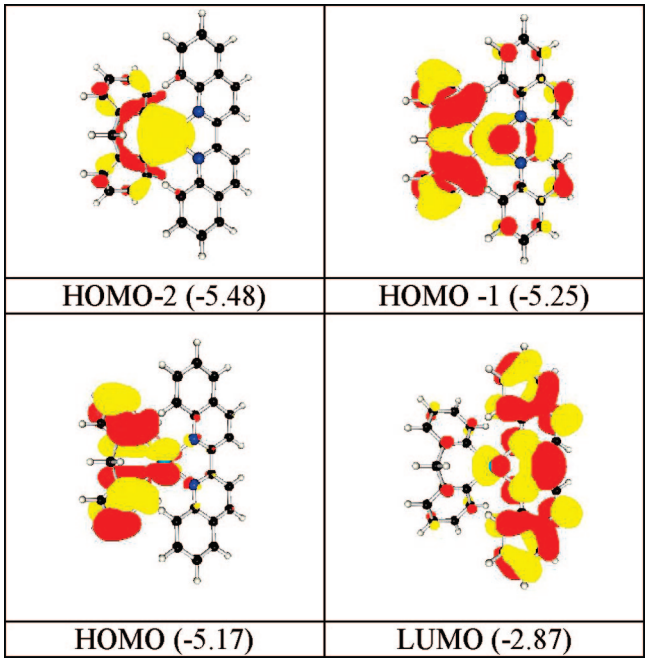

Figure 15. Shapes of relevant orbitals and their energies (eV) for 2,2′-biquinoline compound **16**, calculated using G03/RB3LYP using the SDD basis set for singlet ground state (see Supporting Information for compound **17**).

Synthesis of Precursors for Luminescent Platinum Complexes. Synthesis of 2,2′-Dichlorodiphenylmethanol, 1. This is a slightly modified literature procedure:[34] a 100 mL three-necked round-bottom flask equipped with a stir bar, an addition funnel, and a condenser was charged with Mg turnings (0.924 g, 0.0380 mol), which were activated with a 400 °C heat gun under vacuum for 1 h. To the activated Mg turnings was added dry diethyl ether (25 mL), and a solution containing degassed 1-bromo-2-chlorobenzene (7.00 g, 4.27 mL, 0.0365 mol) in dry ether (15 mL) was added via the addition funnel over a period of 30 to 45 min, while the solution was stirred under reflux. The reaction was then refluxed for an additional 1.5 h or until most of the Mg turnings were in solution. A dry diethyl ether solution (12 mL) containing degassed 2-chlorobenzaldehyde (5.14 g, 4.12 mL, 0.0366 mol) was added dropwise, but rapidly (not streaming). The reaction mixture was refluxed for another 2 h and allowed to stir at room temperature overnight. Stirring may be difficult because of the salt formation. The slurry was treated with 150 mL of 25% NH_4Cl and 25 mL of 3 N HCl. The phases were separated and the aqueous phase was extracted four times with 50 mL of diethyl ether. The combined diethyl ether extracts were washed with 150 mL of distilled water, 125 mL of 10% Na_2SO_3, and 150 mL of distilled water. The diethyl ether solution was dried with $MgSO_4$, filtered, and evaporated in vacuo, yielding a crude yellow oil. This oil was vacuum-distilled, giving the carbinol as a white solid with slightly greenish tinge: bp 128 °C at 0.027 kPa, 46% yield (4.25 g). Carbinol peak confirmed by D_2O exchange in $CDCl_3$. ^1H NMR (200 MHz, $CDCl_3$): δ 7.15−7.45 (8H, m, Ar-H), 6.52 (1H, d, C-H, $J = 3.6$ Hz), 2.57 (1H, d, OH, $J = 4.0$ Hz). ^{13}C NMR (125 MHz, $CDCl_3$): δ 139.49, 133.47, 129.77, 129.25, 128.49, 127.13, 69.84.

Synthesis of 2,2′-Dichlorodiphenylmethane, 2. Iodine (4.71 g, 0.0186 mol), 2,2′-dichlorodiphenylmethanol (4.71 g, 0.0186 mol), and glacial acetic acid (110 mL) were stirred under nitrogen in a 250 mL round-bottomed flask with a condenser for about 15 min. Hypophosphorous acid, H_3PO_2 (50% aqueous, 9.5 mL, 0.092 mol), was added by syringe, and the mixture was heated to 60 °C. The mixture was stirred for 20 h under nitrogen and then diluted with 55 mL of water. The milky white aqueous phase was extracted with two 50 mL portions of hexanes, and the volume was reduced in vacuo. The organic layer was dried over $MgSO_4$ for 24 h and filtered, and solvent was removed under vacuum.[35] If the oil is purple in color, this can be removed by vacuum or washing with solution of aqueous bisulfite (the color is from iodine).[36] A vacuum distillation of the oily product gives a clear oil in 96% yield (4.23 g); impurities remain below 130 °C at 0.020 kPa. ^1H NMR (200 MHz, $CDCl_3$): δ 6.98−7.41 (8H, m, Ar-H), 4.19 (2H, s, CH_2). ^{13}C

(34) Kepler, J. A.; Sparacino, C. M.; Howe, C. R.; Austin, R. D. *J. Labelled Compds Radiopharm.* **1982**, *19*, 271.

(35) Gordon, P. E.; Fry, A. J. *Tetrahedron Lett.* **2001**, *42*, 831.

(36) Fry, A. J. (Wesleyan University) personal communication.

Table 3. Calculated HOMO–LUMO Gap Using G03 at the RB3LYP Level with SDD Atomic Basis Set

metallacycle compound	gas phase HOMO–LUMO gap, hartrees (kcal/mol)[a]	solution phase HOMO–LUMO gap, hartrees (kcal/mol)[b]
2,2′-bipyridine, **8**	0.092 (57.73)	0.118 (74.04)
4,4′-dichloro-2,2′-bipyridine, **9**	0.085 (53.34)	0.109 (68.40)
4,4′-dimethoxy-2,2′-bipyridine, **10**	0.091 (57.10)	0.116 (72.79)
4,4′-bis(dimethylamino)-2,2′-bipyridine, **11**	0.100 (62.75)	0.126 (79.07)
4,4′-di-*tert*-butyl-2,2′-bipyridine, **12**	0.098 (61.50)	0.121 (75.93)
1,10-phenanthroline, **13**	0.094 (58.99)	0.120 (75.30)
2,9-dimethyl-1,10-phenanthroline, **14**	0.098 (61.50)	0.121 (75.93)
3,4,7,8-tetramethyl-1,10-phenanthroline, **15**	0.097 (60.86)	0.125 (78.44)
2,2′-biquinoline, **16**	0.085 (53.34)	0.101 (63.38)
N,N,N′N′-tetramethylethylenediamine, **17**	0.172 (107.93)	0.193 (121.11)

[a] Using singlet ground-state DFT at RB3LYP correlation and SDD basis set. [b] Using singlet ground-state TD-DFT at RB3LYP correlation and SDD basis set with PCM solvent model with acetonitrile (see DFT notes in Experimental Section).

Table 4. Analysis of absorbances for compounds 8–16. Experimental values are listed for comparison with computed (TD-DFT, singlet excitations, G03/RB3LYP, SDD basis set) absorbance data. The three lowest-energy transitions are shown for the TD-DFT computations.

compound	(1 = lowest)	main character MO# → MO#	transition energy/eV (nm)	oscillator strength (*f*)	assignment[d]	experimental λ_{abs}/nm (ϵ /M^{-1} cm^{-1})[a]
8	1	95% S_1 94 → 95[b]	2.52 (491.5)	0.0108	MMLLCT/LLCT	429 (1900)
	2	97% S_1 92 → 95	2.59 (478.3)	0.0014	MLCT	
	3	94% S_1 93 → 95	2.63 (471.2)	0.0920	MMLLCT	
9	1	95% S_1 110 → 111[b]	2.29 (540.5)	0.0118	MMLLCT/LLCT	455 (1330)
	2	97% S_1 108 → 111	2.37 (524.2)	0.0018	MLCT	
	3	94% S_1 109 → 111	2.40 (515.8)	0.0932	MMLLCT	
10	1	95% S_1 110 → 111[b]	2.48 (499.3)	0.0072	MMLLCT/LLCT	411 (7210)
	2	96% S_1 108 → 111	2.56 (484.6)	0.0032	MLCT	
	3	94% S_1 109 → 111	2.57 (481.6)	0.0977	MMLLCT	
11	1	96% S_1 117 → 119	2.78 (446.1)	0.0101	MMLLCT/LLCT	395 (8000)
	2	95% S_1 118 → 119[b]	2.83 (438.1)	0.1389	MMLLCT/LLCT	
	3	98% S_1 116 → 119	2.90 (427.5)	0.0017	MLCT	
12	1	95% S_1 126 → 127[b]	2.62 (473.6)	0.0121	MMLLCT/LLCT	421 (2650)
	2	96% S_1 124 → 127	2.69 (461.7)	0.0017	MLCT	
	3	94% S_1 125 → 127	2.71 (457.9)	0.1031	MMLLCT	
13	1	95% S_1 100 → 101[b]	2.56 (483.8)	0.0084	MMLLCT/LLCT	430 (1733)
	2	90% S_1 98 → 101	2.63 (471.9)	0.0050	MLCT	
		7% S_1 99 → 101	2.63 (471.9)	0.0050	MMLLCT	
	3	83% S_1 99 → 101	2.66 (466.9)	0.0799	MMLLCT	
		7% S_1 98 → 101	2.66 (466.9)	0.0799	MLCT	
		6% S_1 100 → 102	2.66 (466.9)	0.0799	MMLLCT/LLCT	
14	1	95% S_1 108 → 109[b]	2.61 (475.3)	0.0064	MMLLCT/LLCT	423 (2300)
	2	98% S_1 106 → 109	2.64 (469.3)	0.0036	MLCT	
	3	89% S_1 107 → 109	2.69 (461.3)	0.0835	MMLLCT	
		7% S_1 108 → 110	2.69 (461.3)	0.0835	MMLLCT/LLCT	
15	1	93% S_1 116 → 118	2.72(455.1)	0.0050	MMLLCT/LLCT	405 (5500)[c]
	2	56% S_1 115 → 118	2.78 (446.6)	0.0311	MMLLCT	
		33% S_1 116 → 117[b]	2.78 (446.6)	0.0311	MMLLCT/LLCT	
		8% S_1 114 → 118	2.78 (446.6)	0.0311	MLCT	
	3	89% S_1 114 → 118	2.80 (442.6)	0.0047	MLCT	
		5% S_1 116 → 117[b]	2.80 (442.6)	0.0047	MMLLCT/LLCT	
16	1	95% S_1 120 → 121[b]	2.08 (595.9)	0.0064	MMLLCT/LLCT	523 (700)
	2	95% S_1 118 → 121	2.17 (572.4)	0.0042	MLCT	
	3	88% S_1 119 → 121	2.27 (545.4)	0.1487	MMLLCT	

[a] UV–vis spectra data were measured in anhydrous deoxygenated CH_3CN using a quartz cuvette. [b] HOMO–LUMO. [c] Larger error associated in the determination of ϵ (up to ±30%) due to very low solubility. [d] MLCT, metal-to-ligand charge transfer; LLCT, ligand-to-ligand charge transfer; MMLLCT, mixed-metal-ligand-to-ligand charge transfer.

NMR (125 MHz, $CDCl_3$): δ 137.32, 134.63, 130.92, 129.74, 128.10, 127.12, 36.97.

Synthesis of Lithium Pellets Containing 2.5% Sodium, Alloy, 3. In an oven-dried 500 mL flat-bottomed flask fitted with a large stir bar and argon inlet/outlet, lithium chips (1–3 g) containing 0.5% sodium and additional sodium metal (2% w/w) were heated to a boil in anhydrous tetralin (bp 207 °C, 50 mL). The contents were stirred vigorously until all metal had melted, and the temperature was maintained at this level for 15 min. Then the heat was turned off. The contents were allowed to slowly cool to room temperature under vigorous stirring. Under an atmosphere of argon, the tetralin was carefully covered with a layer of pentane; the light lithium rose to the top of the pentane layer. Using a pipet, most of the brownish tetralin solution beneath the pentane was removed. The very small lithium pellets were washed several times with anhydrous pentane and dried under vacuum.[37]

Synthesis of 2,2′-Dilithiodiphenylmethane Solution, 4. The freshly made (as per the method above) Na-enriched Li (0.180 g, 0.025 mol) was cut into pieces using scissors and flattened with a glass bottle (used as a roller) into thin sheets (0.5 cm by 3 cm) of lustrous metal foil, which were then placed in diethyl ether (5 mL) in a one-neck, 100 mL round-bottomed flask (oven-dried) under Ar atmosphere. The flask was fitted with a stir bar and addition funnel and cooled to 0 °C on ice. A solution of 2,2′-dichlorodiphenylmethane (0.5 g, 0.00215 mol) in diethyl ether (9 mL) was added dropwise over a period of 45 min with vigorous stirring under dynamic argon atmosphere. The resulting orange solution was then glass stoppered (under static argon), transferred to a 2 °C refrigerator with power outlets and stir plate, and left to stir vigorously for 20 to 22 h. Under argon atmosphere, at room temperature, the reaction mixture was filtered of excess lithium metal using a 0.2 μm Whatman disk filter and 30 mL glass syringe. The remaining excess Li chips and flask were washed two times with 2 mL of dry ether, the washings were combined, and the 18 mL organolithium solution was stored in a −35 °C freezer (although it is recommended to use organolithium solution as quickly as possible). LiCl salt was isolated and tested via flame test to give a red combustion flame. The concentration of the dilithio compound was determined by a Gilman double titration where separate aliquots (0.5 mL each) were quenched with water and 1,2-dibromoethane and titrated against 0.020000 ± 0.00002 N HCl using phenolphthalein indicator for the neutralization. Yield was calculated to be 80% to 93% organolithium (not necessarily dilithium reagent, as monolithiated reagent can also give a false positive) for this 0.5 g scale. The solution is dark orange and should be stored under argon at −35 °C. Organolithium solutions containing more then 15% basic impurities were rejected.[4,14,38–41]

Synthesis of *cis*-$PtCl_2(SEt_2)_2$, 5. K_2PtCl_4 (4.15 g, 0.0100 mol) was dissolved in 50 mL of water and stirred vigorously in a 100 mL round-bottomed flask to give a deep red solution. Diethyl sulfide (3.61 g, 4.31 mL, 0.0400 mol) was added, and the flask was stoppered. The originally deep red supernatant solution became colorless while a yellow precipitate formed (within 20 min). The mixture was then stirred for an additional 24 h or until the yellow precipitate (trans-isomer), initially formed, dissolves completely. The resulting clear yellow solution is then reduced to dryness, by applying vacuum at 25 °C, to yield a yellow-white precipitate. The isomeric mixture is extracted from the residue, by treatment with a minimum amount of hot benzene (40 mL). The hot solution is filtered on a hot funnel to remove KCl. After filtration, the benzene solution is evaporated to half-volume and cooled in an ice bath, whereupon fine, yellow crystals of the cis-isomer form. The crystals are separated by suction filtration and washed with several 5 mL portions of hexanes to remove any trans-isomer. Yield: 83% (3.71 g). ^{1}H NMR (200 MHz, $CDCl_3$, diastereotopic methylene hydrogens denoted as H_a/H_b): δ 3.10–3.43 (4H, m, S-H_a), 2.43–2.94 (4H, m, S-H_b), 1.40 (12H, t, CH_3, J = 7.4 Hz). ^{13}C NMR (125 MHz, $CDCl_3$): δ 32.36, 13.26.[42]

Synthesis of $\{[H_2C(C_6H_4)_2]Pt(SEt_2)\}_n$ (n = 2, 3), 6. Solid $PtCl_2(SEt_2)_2$ (**5**) (0.307 g, 0.688 mmol) was added to a dark orange solution of 0.130 M 2,2′-dilithiodiphenylmethane (5.60 mL, 0.728 mmol) in diethyl ether at room temperature. The mixture was stirred for 4 h at ambient temperature under static argon to give a light brown precipitate. Then 7.00 mL of water (solubility of LiCl 84.5g/100 mL of H_2O at 25 °C[43]) was added to quench the solution, and the volatiles were evaporated under vacuum to give a brown sludge in water. The mixture was then extracted with 3 × 45 mL of dichloromethane, and the volume was reduced under vacuum and dried over $MgSO_4$ overnight. (If the organolithium solution is of high quality, i.e., less than 15% basic impurity, upon the first extraction of the aqueous phase, a white insoluble powder can be seen dropping to the bottom of the extraction funnel. This is the desired product, and use of $MgSO_4$ should be skipped, as this insoluble product will be lost during the filtration of $MgSO_4$.) The light brown solution was then filtered, and $MgSO_4$ residue was washed with two 45 mL portions of dichloromethane, as the oligomer is appreciably soluble in dichloromethane. The washings were combined and dried in vacuo to yield a dark brown oil. Then 2 mL of acetone was added to reveal a white powder. The solid was isolated by centrifugation and washed with a minimal amount (~1 mL) of cold acetone. The white solid was dried in vacuo and placed in a −35 °C freezer. The product was obtained in 52% (162 mg) yield. Yield and overall procedure are similar to what has been reported for other dialkylsulfide-bridged oligomers of diarylplatinum complexes.[44–46] NMR spectroscopy showed that **6** was present in two forms, $\mathbf{6}_{(major)}$ and $\mathbf{6}_{(minor)}$, in a ratio of 78:22 (per Pt). The two distinct species are assigned as cyclic oligomers with n = 2 or 3. A mixture of cyclic dimer and trimer has been reported for the similar $[PtPh_2(S(CH_3)_2)]_n$ (n = 2, 3), where both the dimer and the trimer have been crystallographically characterized.[47] No attempt has been made here to assign the individual nuclearity of the major and the minor species of **6**.

$\mathbf{6}_{(major)}$. ^{1}H NMR (500 MHz, C_6D_6): δ 6.93−7.32 (m, aromatic region overlap with aromatic region of $\mathbf{6}_{(minor)}$), 4.46 (1 H, d, CH_2, J= 14.0 Hz), 3.68 (1 H, d, CH_2, J= 14.0 Hz), 2.60 (2 H, m, S-CH_2CH$_3$), 2.28 (2 H, m, S-CH_2CH$_3$), 1.31 (6 H, t, S-CH$_2$CH_3, J= 7.5 Hz). $\mathbf{6}_{(minor)}$ ^{1}H NMR (500 MHz, C_6D_6): δ 6.93−7.32 (m, aromatic region over lap with aromatic region of $\mathbf{6}_{(major)}$), 4.38 (1 H, d, CH_2, J = 13.5 Hz), 3.62 (1 H, d, CH_2, J = 14.0 Hz), 2.92 (2 H, m, S-CH_2CH$_3$), 2.09 (2 H, m, S-CH_2CH$_3$), 1.58 (3 H, t, S-CH$_2$CH_3, J = 7.0 Hz), 1.02 (3H, t, S-CH$_2$CH_3, J = 7.0 Hz). ^{13}C NMR (125 MHz, $CDCl_3$) of $\mathbf{6}_{(major)}$ only: δ 146.07, 143.21, 133.86, 126.08, 124.74, 123.75, 50.28, 31.19, 12.63. m/z [MALDI-TOF-MS]: 451.3; predicted for monomeric (gas-phase ion) $C_{17}H_{20}Pt_1S_1$, 451.1. The isotope pattern (450.3, 82%; 451.3, 100%; 452.3, 85%; 453.3, 19%; 454.3, 23%; 455.3, 4%) is in perfect agreement with the pattern predicted for $C_{17}H_{20}Pt_1S_1$ (see Supporting Information, Figures S13 and S14).

Solution Data for 6b and NOE Assignment of Nonequivalent Methylene (CH_2) Protons. An excess (approximately 5 to 10 equiv) of SEt_2 was added to a stirred/shaken suspension of compound **6** in approximately 480 μL of CD_2Cl_2 to give the highly soluble, monomeric $Pt(SEt_2)_2(CH_2(C_6H_4)_2)$, **6b**, after gentle reflux for 4 min. ^{1}H NMR (500 MHz, CD_2Cl_2): δ 7.38 (2H, m, Ar-H, $^3J_{PtH}$ = 73 Hz), 7.01 (2H, m, Ar-H, $^3J_{PtH}$ = unresolved broad base), 6.69–6.87 (4H, m, Ar-H), 4.08 (1H, d, C-H, $^4J_{PtH}$ = 16.0 Hz, J = 13.5 Hz), 3.37 (1H, d, C-H, $^4J_{PtH}$ = unresolved, broad base, J = 13.5 Hz), 2.78–2.85 (4H, m, coordinated S-CH_2CH$_3$), 2.63–2.71 (4H, m, coordinated S-CH_2CH$_3$), 2.53 (18H excess, free S-CH_2CH$_3$, q, J = 7.4 Hz), 1.28 (12H, t, coordinated S-CH$_2$CH_3, J = 8.0 Hz), 1.24 (27 H excess, free S-CH$_2$CH_3, t, J = 8.0 Hz). ^{13}C NMR (125 MHz, CD_2Cl_2) δ 149.12, 145.56, 136.32, 125.57, 124.42, 122.67, 51.20, 28.91 (S-CH_2CH$_3$ of coordinated SEt_2), 25.37 (S-CH_2CH$_3$ of free SEt_2), 14.93 (S-CH$_2$CH_3 of coordinated SEt_2), 13.35 (S-

(37) Keese, R.; Brändle, M. P.; Trevor, P. T. *Practical Organic Chemistry: A Students Guide,* Chichester; Hoboken, NJ.: Wiley, **2006**, P. 135.
(38) Gilman, H.; Haubein, A. H. *J. Am Chem. Soc.,* **1944**, *66*, 1515.
(39) Wakefield, B. J. *Organolithium Methods*, Academic Press; London, **1988**.
(40) Wakefield, B. J. *The Chemistry of Organolithium Compounds*. Pergamon Press; New York, **1972**.
(41) Shriver, D. F. *The Manipulation of Air-Sensitive Compounds*. Wiley-Interscience Publication; New York, **1986**.
(42) Kauffman, G. B.; Cowan, D. O. *Inorg. Synth.*, **1966**, *6*, 211.
(43) CRC Handbook of Chemistry and Physics, 87th Edition. 2006-2007. http://www.hbcpnetbase.com/ Accessed September 2007.
(44) Lacabra, M. A. C.; Canty, A. J.; Lutz, M.; Patel, J.; Spek, A. L.; Sun, H.; van Koten, G. *Inorg. Chim. Acta,* **2002**, *327*, 15.
(45) Plutino, M. R.; Monsù Scolaro, L.; Albinati, A.; Romeo, R. *J. Am. Chem. Soc.,* **2004**, *126*, 6470.
(46) Steele, B. R.; Vrieze, K. *Transition Met. Chem.,* **1977**, *2*, 140.
(47) Song, D.; Wang, S. *J. Organomet. Chem.* **2002**, *648*, 302.

CH_2CH_3 of free SEt_2). NOESY Spectra taken at 0 °C. Irradiation of the methylene peak at 3.37 ppm leads to an NOE observation at 4.08 and 7.01 ppm. Irradiation of the methylene peak at 4.08 ppm leads to an NOE observation at 3.37 ppm. Irradiation of the aromatic peak at 7.01 ppm leads to an NOE observation at 3.37 ppm.

Synthesis of 4,4′-Bis(dimethylamino)-2,2′-bipyridine (7). This ligand has been previously synthesized and fully characterized, but the synthesis was low-yielding (23%).[33] We obtained it in improved yield by using a modification of a literature procedure for substituted pyridines.[32] 4,4′-Dichloro-2,2′-bipyridine (0.250 g, 0.0011 mol) was refluxed with stirring in dimethylformamide (4.00 mL, 3.78 g, 0.052 mol) at 165 °C for 18 h in a 25 mL Pyrex reaction vessel. Removal of excess DMF was accomplished by evacuation. Dissolution of the hydrochloride salt was done by adding a saturated sodium bicarbonate solution to the precipitate and shaking vigorously in an extraction funnel to yield an insoluble product. The insoluble product was triturated, filtered, washed with copious amounts of distilled water, and dried in vacuo to yield a light beige powder in 58% yield (156 mg). ^{1}H NMR (200 MHz, $(CD_3)_2SO$): in excellent agreement with literature,[33] δ 8.19 (2H, d, Ar-H, $J = 5.8$ Hz), 7.66 (2H, d, Ar-H, $J = 2.4$ Hz), 6.63 (2H, dd, Ar-H, $J = 2.6$, 6.0 Hz), 3.01 (12H, s, ArN-CH_3). ^{13}C NMR (125 MHz, $(CD_3)_2SO$): δ 155.89, 154.78, 148.79, 106.74, 103.04, 38.90 (sh on DMSO peak).

Synthesis of Monomeric Luminescent Platinum Complexes. Synthesis of Pt($CH_2(C_6H_4)_2$)(diimine) 8–17. The Pt($CH_2(C_6H_4)_2$)(diimine) complexes were prepared by displacement of the diethylsulfide ligands to give the monomeric metallacyclic diimine complexes. The reactions were performed on NMR scales (8 to 26 mg), and conversion was quantitative by 500 MHz ^{1}H NMR, but isolated yields varied from 88 to 96%.

Synthesis of Pt($CH_2(C_6H_4)_2$)(2,2′-bipyridine), 8. To a suspension of $\{[H_2C(C_6H_4)_2]Pt(SEt_2)\}_n$ ($n = 2$), **6** (8.00 mg, 0.00887 mmol), in 560 uL of C_6D_6 in a J. Yonge NMR tube was added 2,2-bipyridine (2.77 mg, 0.0177 mmol). The solution was sonicated for 1 min and heated to reflux for 5 min while a color change occurred. The highly colored product was initially (at elevated temperature) dissolved and then slowly crystallized upon cooling. The reaction was monitored to completion by ^{1}H NMR using the appearance of free diethylsulfide peaks at 2.26 ppm (4H, q, $^3J = 7.0$ Hz) and 1.05 ppm (6H, t, $^3J = 7.5$ Hz) and the disappearance of coordinated diethylsulfide peaks as indicative of reaction progress. The solution was dried under reduced pressure to remove free SEt_2 and solvent to reveal a yellow product in quantitative yield. Product is mostly insoluble in organic solvents. Analytically pure samples can be achieved by washing the insoluble product in copious amounts of benzene and hexanes. ^{1}H NMR (500 MHz, $(CD_3)_2SO$): δ 8.92 (2H, d, ArN-H, $J = 5.5$ Hz), 8.70 (2H, d, ArN-H, $J = 8.0$ Hz), 8.37 (2H, t, ArN-H, $J = 8.0$ Hz), 7.79 (2H, t, ArN-H, $J = 7.0$ Hz), 7.30 (2H, d, Ar-H, $^3J_{PtH}$ = broad base (unresolved), $J = 7.5$ Hz), 6.98 (2H, d, Ar-H, $J = 7.0$ Hz), 6.86 (2H, t, Ar-H, $J = 7.0$ Hz), 6.77 (2H, t, Ar-H, $J = 7.5$ Hz), 3.98 (2H, d, CH_2, $J = 13.0$ Hz), 3.36 (1H, d, CH_2, J = unresolved). ^{13}C NMR (125 MHz, $(CD_3)_2SO$): δ 155.55, 149.17, 147.48, 145.72, 144.13, 138.76, 137.37, 127.23, 124.10, 123.72, 121.59, 50.56. Anal. Calcd for $PtC_{23}H_{18}N_2 \cdot \frac{1}{2}H_2O$: C, 52.47; H, 3.64; N, 5.32. Found: C, 52.80; H, 3.43; N, 4.86.

Synthesis of Pt($CH_2(C_6H_4)_2$)(4,4′-dichloro-2,2′-bipyridine), 9. This complex was prepared using the method described for Pt($CH_2(C_6H_4)_2$)(2,2′-bipyridine) (**8**) to give an orange precipitate in quantitative yield. Analytically pure samples can be achieved by washing the moderately soluble product in copious amounts of benzene and hexanes and precipitation from a slowly cooled, supersaturated acetonitrile solution. ^{1}H NMR (500 MHz, $(CD_3)_2SO$): δ 8.98 (2H, s, ArN-H), 8.83 (2H, d, ArN-H, $J = 6.0$ Hz), 7.95 (2H, dd, ArN-H, $J = 1.75$, 5.15 Hz), 7.27 (2H, d, Ar-H, $^3J_{PtH}$ = broad base (unresolved), $J = 7.0$ Hz), 6.98 (2H, d, Ar-H, $J = 7.0$ Hz), 6.85 (2H, t, Ar-H, $J = 7.0$ Hz), 6.77 (2H, t, Ar-H, $J = 7.0$ Hz), 3.96 (1H, d, CH_2, $J = 13.0$ Hz), 3.32 (1H, d, CH_2, J = unresolved). ^{13}C NMR (125 MHz, $(CD_3)_2SO$): δ 156.40, 150.10, 147.33, 145.10, 144.98, 137.12, 127.79, 127.75, 124.67, 124.19, 121.78, 50.40. Anal. Calcd for $PtC_{23}H_{16}N_2Cl_2$: C, 47.11; H, 2.75; N, 4.78. Found: C, 47.03; H, 2.95; N, 5.17.

Synthesis of Pt($CH_2(C_6H_4)_2$)(4,4′-dimethoxy-2,2′-bipyridine), 10. This complex was prepared using the method described for Pt($CH_2(C_6H_4)_2$)(2,2′-bipyridine) (**8**) to give a yellow-green precipitate in quantitative yield. Analytically pure samples can be achieved by washing insoluble products in copious amounts of benzene and hexanes. ^{1}H NMR (500 MHz, $(CD_3)_2SO$): δ 8.66 (2H, d, ArN-H, $J = 6.5$ Hz), 8.26 (2H, s, ArN-H), 7.37 (2H, dd, ArN-H, $J = 1.5$, 5.70 Hz), 7.26 (2H, d, Ar-H, $^3J_{PtH}$ = broad base (unresolved), $J = 7.0$ Hz), 6.95 (2H, d, Ar-H, $J = 7.0$ Hz), 6.80 (2H, t, Ar-H, $J = 7.0$ Hz), 6.73 (2H, t, Ar-H, $J = 7.0$ Hz), 4.01 (6H, s, OCH_3), 3.95 (1H, d, CH_2, $J = 13.0$ Hz), 3.30 (1H, d, CH_2, J = unresolved). ^{13}C NMR (125 MHz, $(CD_3)_2SO$): δ 166.78, 157.30, 150.29, 147.41, 146.02, 137.26, 127.75, 123.94, 121.24, 112.50, 110.39, 56.70, 37(sh on DMSO solv peak). Anal. Calcd for $PtC_{25}H_{22}N_2O_2 \cdot \frac{1}{2}H_2O$: C, 51.19; H, 3.95; N, 4.78. Found: C, 51.24; H, 3.92; N, 4.22.

Synthesis of Pt($CH_2(C_6H_4)_2$)(4,4′-bis(dimethylamino)-2,2′-bipyridine), 11. This complex was prepared using the method described for Pt($CH_2(C_6H_4)_2$)(2,2′-bipyridine) (**8**) to give a greenish-yellow precipitate in quantitative yield. Analytically pure samples can be achieved by washing insoluble products in copious amounts of benzene and hexanes. ^{1}H NMR (500 MHz, $(CD_3)_2SO$): δ 8.31 (2H, d, ArN-H, $J = 6.5$ Hz), 7.59 (2H, d, ArN-H, $J = 2.5$ Hz), 7.24 (2H, d, Ar-H, $J = 7.0$ Hz), 6.90 (2H, d, Ar-H, $J = 7.0$ Hz), 6.86 (2H, dd, ArN-H, $J = 3.0$, 6.75 Hz), 6.75 (2H, t, Ar-H, $J = 6.0$ Hz), 6.69 (2H, t, Ar-H, $J = 7.5$ Hz), 3.91 (1H, d, CH_2, $J = 13.0$ Hz), 3.27 (1H, d, CH_2, $J = 13.5$ Hz), 3.15 (12H, s, CH_3). Too insoluble to obtain ^{13}C. Anal. Calcd for $PtC_{27}H_{28}N_4 \cdot 2H_2O$: C, 50.70; H, 5.04; N, 8.76. Found: C, 50.74; H, 4.81; N, 8.34.

Synthesis of Pt($CH_2(C_6H_4)_2$)(4,4′-di-*tert*-butyl)-2,2′-bipyridine), 12. This complex was prepared using the method described for Pt($CH_2(C_6H_4)_2$)(2,2′-bipyridine) (**8**) to give a green-yellow precipitate in quantitative yield. Analytically pure samples can be achieved by washing insoluble products in copious amounts of benzene and hexanes. ^{1}H NMR (500 MHz, $(CD_3)_2SO$): δ 8.80 (2H, d, ArN-H, $J = 6.0$ Hz), 8.65 (2H, d, ArN-H, $J = 1.5$ Hz), 7.77 (2H, dd, ArN-H, $J = 2.0$, 6.0 Hz), 7.27 (2H, d, Ar-H, $J = 7.5$ Hz), 6.96 (2H, d, Ar-H, $J = 6.5$ Hz), 6.83 (2H, t, Ar-H, $J = 7.5$ Hz), 6.75 (2H, t, Ar-H, $J = 7.5$ Hz), 3.95 (1H, d, CH_2, $J = 13.0$ Hz), 3.31 (1H, d, CH_2, J = unresolved), 1.42 (18H, s, CH_3). ^{13}C NMR (125 MHz, $(CD_3)_2SO$): δ 162.64, 155.49, 148.91, 147.42, 146.12, 137.39, 124.03, 123.97, 123.86, 121.42, 120.86, 50.61, 35.75, 29.91. Anal. Calcd for $PtC_{31}H_{34}N_2 \cdot \frac{1}{2}H_2O$: C, 58.29; H, 5.52; N, 4.39. Found: C, 58.46; H, 5.89; N, 4.36.

Synthesis of Pt($CH_2(C_6H_4)_2$)(1,10-phenanthroline), 13. This complex was prepared using the method described for Pt($CH_2(C_6H_4)_2$)(2,2′-bipyridine) (**8**) to give a yellow precipitate in quantitative yield. Analytically pure samples can be achieved by washing insoluble products in copious amounts of benzene and hexanes and precipitation of slowly cooled, supersaturated acetonitrile solutions. ^{1}H NMR taken at 30 °C (500 MHz, $(CD_3)_2SO$): δ 9.30 (2H, dd, ArN-H, $J = 1.0$, 5.25 Hz), 8.99 (2H, dd, ArN-H, $J = 1.0$, 8.0 Hz), 8.29 (2H, s, ArN-H), 8.15 (2H, dd, ArN-H, $J = 5.0$, 8.0 Hz), 7.46 (2H, d, Ar-H, $J = 7.5$ Hz), 7.03 (2H, d, Ar-H, $J = 8.0$ Hz), 6.92 (2H, t, Ar-H, $J = 7.0$ Hz), 6.81 (2H, t, Ar-H, $J = 7.5$ Hz), 4.04 (1H, d, CH_2, $J = 13.5$ Hz), 3.39 (1H, d, $J = 13.5$ Hz). Too insoluble to obtain ^{13}C. Anal. Calcd for $PtC_{25}H_{18}N_2 \cdot \frac{1}{2}H_2O$: C, 54.54; H, 3.48; N, 5.09. Found: C, 54.56; H, 3.48; N, 5.15.

Synthesis of Pt($CH_2(C_6H_4)_2$)(2,9-dimethyl-1,10-phenanthroline), 14. This complex was prepared using the method described for Pt($CH_2(C_6H_4)_2$)(2,2′-bipyridine) (**8**) to give a yellow precipitate in quantitative yield. Analytically pure samples can be achieved by washing insoluble products in copious amounts of benzene and

hexanes. ^{1}H NMR (500 MHz, $(CD_3)_2SO$): δ 8.76 (2H, d, ArN-H, J = 8.0 Hz), 8.15 (2H, s, ArN-H), 7.91 (2H, d, ArN-H, J = 8.5 Hz), 6.98 (2H, d, Ar-H, J = 7.0 Hz), 6.76 (2H, d, Ar-H, J = 7.5 Hz), 6.65 (2H, t, Ar-H, J = 7.0 Hz), 6.55 (2H, t, Ar-H, J = 7.0 Hz), 4.35 (1H, d, CH_2, J = 13.0 Hz), 3.40 (1H, d, J = 13.0 Hz), 2.35 (6H, s, CH_3). ^{13}C NMR (125 MHz, $(CD_3)_2SO$): δ 161.73, 147.12, 146.67, 138.28, 137.46, 137.28, 127.47, 125.95, 124.19, 122.60, 121.41, 119.98, 58.16, 28.25. Anal. Calcd for $PtC_{27}H_{22}N_2$: C, 56.94; H, 3.89; N, 4.92; S, 0. Found: C, 56.47; H, 3.81; N, 4.81; S, <0.2. See Figure 5 and Supporting Information for details on the crystal structure.

Synthesis of Pt($CH_2(C_6H_4)_2$)(3,4,7,8-tetramethyl-1,10-phenanthroline), 15. This complex was prepared using the method described for Pt($CH_2(C_6H_4)_2$)(2,2′-bipyridine) (**8**) to give a yellow precipitate in quantitative yield. ^{1}H NMR spectra were taken at 60 °C to aid dissolution. The resulting heat coalesces the inequivalent methylene CH_2 to broadened peaks, probably due to ring flipping at elevated temperatures. Analytically pure samples can be achieved by washing insoluble products in copious amounts of benzene and hexanes and precipitation of slowly cooled, supersaturated acetonitrile solutions. ^{1}H NMR (500 MHz, $(CD_3)_2SO$): δ 9.03 (2H, s, ArN-H), 8.40 (2H, s, ArN-H), 7.44 (2H, d, Ar-H, J = 6.0 Hz), 7.01 (2H, d, Ar-H, J = 8.5 Hz), 6.91 (2H, t, Ar-H, J = 7.5 Hz), 6.80 (2H, t, Ar-H, J = 7.0 Hz), 4.0 (1H, s br, CH_2), 3.1 (1H, s br, CH_2), 2.75 (6H, s, ArN-CH_3), 2.55 (6H, s, ArN-CH_3). Too insoluble to obtain ^{13}C. Anal. Calcd for $PtC_{29}H_{26}N_2$: C, 58.28; H, 4.39; N, 4.69. Found: C, 58.58; H, 4.38; N, 4.69.

Synthesis of Pt($CH_2(C_6H_4)_2$)(2,2′-biquinoline), 16. This complex was prepared using the method described for Pt($CH_2(C_6H_4)_2$)(2,2′-bipyridine) (**8**) to give a purple precipitate in quantitative yield. It required 40 min more for complete substitution to occur, with respect to most other bipyridine substitutions. Using 3 equiv of 2,2′-biquinoline with respect to the oligomer ensures faster and more complete substitution. Analytically pure samples can be achieved by washing insoluble products in copious amounts of benzene and hexanes and precipitation of slowly cooled, supersaturated acetonitrile solutions. ^{1}H NMR (500 MHz, $(CD_3)_2SO$): δ 9.07 (2H, d, ArN-H, J = 8.5 Hz), 8.96 (2H, d, ArN-H, J = 8.5 Hz), 8.20 (2H, d, ArN-H, J = 7.5 Hz), 7.77 (2H, d, Ar-H, J = 8.5 Hz), 7.67 (2H, t, ArN-H, J = 7.5 Hz), 7.37 (2H, t, ArN-H, J = 7.0 Hz), 7.07 (2H, d, Ar-H, J = 7.0 Hz), 6.62 (2H, t, Ar-H, J = 7.0 Hz), 6.23 (2H, t, Ar-H, J = 7.0 Hz), 6.10 (2H, d, ArN-H, J = 7.0 Hz), 4.65 (1H, d, CH_2, J = 12.5 Hz), 3.56 (1H, d, CH_2, J = 13.0 Hz). ^{13}C NMR (125 MHz, $(CD_3)_2SO$): δ 156.92, 155.29, 147.23, 146.57, 136.97, 136.64, 130.16, 129.38, 128.16, 128.04, 127.42, 125.30, 123.45, 123.34, 118.84, 50.25. Anal. Calcd for $PtC_{31}H_{22}N_2 \cdot \frac{1}{2}H_2O$: C, 59.42; H, 3.70; N, 4.47. Found: C, 59.64; H, 3.66; N, 4.56.

Synthesis of Pt($CH_2(C_6H_4)_2$)(*N,N,N′N′*-tetramethylethylenediamine), 17. This complex was prepared using the method described for Pt($CH_2(C_6H_4)_2$)(2,2′-bipyridine) (**8**) to give a white precipitate in quantitative yield. This complex is very soluble in most organic solvents and was purified by recrystallization by slow evaporation in benzene. ^{1}H NMR (200 MHz, $CDCl_3$): δ 7.37 (2H, m, Ar-H, $^3J_{Pt\text{-}H}$ = 74.0 Hz), 6.98 (2H, m, Ar-H, $^3J_{PtH}$ = unresolved broad base), 6.75–6.67 (4H, m, Ar-H), 4.16 (1H, d, CH_2, J = 13.0 Hz, $^4J_{Pt\text{-}H}$ = 19.2 Hz), 3.35 (1H, d, CH_2, J = 13.0 Hz, $^4J_{Pt\text{-}H}$ = 11.2 Hz), 2.88 (6H, s, CH_3, $^3J_{Pt\text{-}H}$ = 18.0 Hz), 2.59 (4H, s, CH_2, $^3J_{Pt\text{-}H}$ = 11.6 Hz), 2.39 (6H, s, CH_3, $^3J_{Pt\text{-}H}$ = 25.2 Hz). ^{13}C NMR (125 MHz, $CDCl_3$): δ 147.82, 140.82, 135.79, 124.60, 123.66, 121.67, 61.94, 51.64, 50.85, 49.40. Anal. Calcd for $PtC_{19}H_{26}N_2 \cdot \frac{1}{2}H_2O$: C, 46.91; H, 5.59; N, 5.76. Found: C, 46.95; H, 5.96; N, 5.37.

Spectroscopic Characterization. UV–vis spectra were obtained on an OLIS-14 (upgraded Cary-14) spectrophotometer with solution concentrations in the 0.02 to 0.07 mM range (see Supporting Information), using 1 cm path-length SUPRASIL QS-110 matching quartz cuvettes. The Windows NT-based computer controlled the UV–vis spectrophotometer with OLIS Spectral Works software version 4.3 with no digital filtering and lamp change occurring at 385 nm. Emission spectra were obtained on a Fluoromax-4 fluorescence spectrofluorometer equipped with 150 W xenon, continuous output, ozone-free lamp and Hamamatsu R928P photomultiplier tube detector. Powders were suspended in a minimal amount of dry hexanes and placed on glass slides during which solvent evaporation furnished the self-adhesive samples to the glass microscope slides. Room-temperature emissions of the solid sample were collected with the glass slide at 45°, reflecting the original light source opposite of the detector. The emission spectra were corrected for the detector sensitivity in the region below 12500 cm^{-1} (800 nm) and calibrated with anthracene standard (emission).

Electrochemical Measurements. Cyclic voltammograms were obtained using a BASi Epsilon electrochemical workstation. The electrochemical cell consisted of a platinum wire auxiliary electrode, nonaqueous Ag/Ag^+ reference electrode, and platinum disk working electrode. TBAHFP (0.1 M) in degassed, low-water (8.7 ppm) acetonitrile was used as the electrolyte. Potentials reported are referenced relative to the freshly sublimed internal standard, ferrocene/ferrocenium (Fc/Fc^+), the reversible redox potential for which is referenced as zero. The nonaqueous electrode was filled with 0.1 M TBAHFP and 0.01 M $AgNO_3$ solution in acetonitrile. Compound solutions were made as 0.001 M acetonitrile solutions (DMF solution for insoluble species) and contained electrolyte solution as well. This decreases the initial concentration of the platinum solution slightly. Analysis was performed in a dry glovebox (Ar atmosphere). The positive feedback *iR* compensation circuitry of the potentiostat was employed; the reversible separation of the anodic and cathodic peaks for the Cp_2Fe oxidation was 58–71 mV in acetonitrile using BASi Epsilon EC software version 1.60.70_XP, BASi ComServer Ver. 3.09, and Firmware Ver. 1.50.

X-Ray Crystallography. Crystal Structure of Pt($CH_2(C_6H_4)_2$)-(2,9-dimethyl-1,10-phenanthroline), 14. A crystalline sample of [$H_2C(C_6H_4)_2$]Pt(2,9-dimethyl-1,10-phenanthroline), compound **14**, was obtained from DMSO-d_6 solvent, when a hot solution was allowed to cool to room temperature. Crystals were obtained as orange blocks. $C_{27}H_{22}N_2Pt$, M_r = 569.56, orthorhombic, space group *Pnma*, a = 19.8057(2) Å, b = 18.9645(7) Å, c = 5.3313(4) Å; V = 2002.46(17) Å^3, Z = 4, ρ_{calc} = 1.889 Mg/m^3, Mo Kα radiation (λ = 0.71073 Å), crystal dimensions 0.10 × 0.06 × 0.03 mm^3, A total of 11 446 reflections were collected on a Nonius Kappa CCD area detector at 150(2) K, of which 2349 were independent. The structure was solved by direct methods and refined on F^2 using the SHELXTL (version 6.12) software package. Final residuals: R_1 = 0.0357 ($I > 2\sigma(I)$), wR_2 = 0.0855 (all data). Further details of the crystal structure investigations may be obtained from the Cambridge Crystallographic Data Centre, on quoting the depository number CCDC 658 451.

Density Functional Theory (DFT) and Time-Dependent Density Functional Theory Calculations (TD-DFT). DFT calculations were performed using Gaussian 03W[48] using the restricted

(48) Frisch, M. J.; Trucks, G. W.; Schlegel, H. B.; Scuseria, G. E.; Robb, M. A.; Cheeseman, J. R.; Montgomery, J. A.; , Vreven, T., Jr.; Kudin, K. N.; Burant, J. C.; Millam, J. M.; Iyengar, S. S.; Tomasi, J.; Barone, V.; Mennucci, B.; Cossi, M.; Scalmani, G.; Rega, N.; Petersson, G. A.; Nakatsuji, H.; Hada, M.; Ehara, M.; Toyota, K.; Fukuda, R.; Hasegawa, J.; Ishida, M.; Nakajima, T.; Honda, Y.; Kitao, Nakai, O.; Klene, M.; Li, X.; Knox, J. E.; Hratchian, H. P.; Cross, J. B.; Bakken, V.; Adamo, C.; Jaramillo, J.; Gomperts, R.; Stratmann, R. E.; Yazyev, O.; Austin, A. J.; Cammi, R.; Pomelli, C.; Ochterski, J. W.; Ayala, P. Y.; Morokuma, K.; Voth, G. A.; Salvador, P.; Dannenberg, J. J.; Zakrzewski, V. G.; Dapprich, S.; Daniels, A. D.; Strain, M. C.; Farkas, O.; Malick, D. K.; Rabuck, A. D.; Raghavachari, K.; Foresman, J. B.; Ortiz, J. V.; Cui, Q.; Baboul, A. G.; Clifford, S.; Cioslowski, J.; Stefanov, B. B.; Liu, G.; Liashenko, A.; Piskorz, P.; Komaromi, I.; Martin, R. L.; Fox, D. J.; Keith, T.; Al-Laham, M. A.; Peng, C. Y.; Nanayakkara, A.; Challacombe, M.; Gill, P. M. W.; Johnson, B.; Chen, W.; Wong, M. W.; Gonzalez, C.; Pople, J. A. *Gaussian 03*, Revision D.01; Gaussian, Inc.: Wallingford, CT, 2004.

B3LYP[26] correlation and SDD atomic basis set with effective core potentials (ECP)[49] as implemented in the Gaussian 03 software. The SDD basis set is the combination of the Huzinaga–Dunning double-ζ basis set[50] on lighter elements with the Stuttgart−Dresden relativistic effective core potential (RECP) basis set combination[51] on platinum. The HOMO (highest occupied molecular orbital) and LUMO (lowest unoccupied molecular orbital) energies were determined using minimized singlet geometries to approximate the ground state. After minimization, vibrational analysis was performed at the same level of calculation to determine if imaginary frequencies were present. Compounds **8** to **17** showed no imaginary frequencies. TD-DFT calculations were performed at minimized singlet structures at the restricted B3LYP[26] level using the SDD[49–51] basis set in order to predict their low-energy absorptions. Considering the differences of the absorption behaviors in gas and solution, the solvent effects of CH_3CN were taken into account by means of the polarizible continuum model (PCM),[52] as implemented in the Gaussian 03 software using default settings. TD-DFT data were analyzed using SWizard software Ver. 4.4.[53] Molecular orbital visualizations were creating using Facio Version 10.9.9 using an iso-value of 0.02 unless otherwise stated.[54]

Acknowledgment. Funding by the Natural Science and Engineering Research Council (NSERC) of Canada, the Canadian Foundation of Innovation, and the University of Toronto (Connaught Foundation) is gratefully acknowledged. We thank Dr. Gord Hamer and Dr. Peter Mitrakos for assistance with NMR spectroscopy. We would like to acknowledge valuable discussions with Professors Robert H. Morris and Datong Song. We thank Mr. Baoxu Liu and Professor Claudiu Gradinaru for the acquisition of the emission spectra.

Supporting Information Available: X-ray crystallographic data for **14** (CIF) and additional orbital pictures, geometry-optimized structures, as well as additional crystallographic data, cyclic voltammograms, spectroscopic information, and correlation graphs (PDF). The CIF may be obtained, free of charge, from the Cambridge Crystallographic Data Centre, on quoting the depository number CCDC 658 451. Both the CIF and the PDF are available free of charge via the Internet at http://pubs.acs.org.

OM700997V

(49) Hay, P. J.; Wadt, W. R. *J. Chem. Phys.,* **1985**, *82*, 270.
(50) Dunning, T. H., Jr.; Hay, P. J. *Modern Theoretical Chemistry*; Editor, Schaefer, H. F.; Plenum: New York, 1976; Vol. 3, p 1.
(51) Dolg, M. Effective Core Potentials. In *Modern Methods and Algorithms of Quantum Chemistry*; John von Neumann Institute for Computing: Jülich, 2000, Vol. 1, p 479.
(52) (a) Cossi, M.; Scalamni, G.; Regar, N.; Barone, V. *J. Chem. Phys.* **2002**, *117*, 43. (b) Barone, V.; Cossi, M. *J. Chem. Phys.* **1997**, *107*, 3210.
(53) Gorelsky, S. I. *SWizard* program, http://www.sg-chem.net, University of Ottawa, Canada, 2007.
(54) Suenaga, M. Kyushu University, Japan. http://www1.bbiq.jp/zzzfelis/Facio.html.